JOHANN WOLFGANG VON GOETHE UNIVERSITÄT

BACHELOR THESIS

Determining the order of the phase transition in a Polyakov-loop model

Author:
Felix MÖLLER

Main supervisor:
Prof. Owe PHILIPSEN
Secondary supervisor:
Prof. Marc WAGNER

01.09.2021

Selbstständigkeitserklärung

Erklärung nach §30 (12) Ordnung für den Bachelor- und den Masterstudiengang

Hiermit erkläre ich, dass ich die Arbeit selbstständig und ohne Benutzung anderer als der angegebenen Quellen und Hilfsmittel verfasst habe. Alle Stellen der Arbeit, die wörtlich oder sinngemäß aus Veröffentlichungen oder aus anderen fremden Texten entnommen wurden, sind von mir als solche kenntlich gemacht worden. Ferner erkläre ich, dass die Arbeit nicht - auch nicht auszugsweise - für eine andere Prüfung verwendet wurde.

Unterschrift: _____

Datum: _____

JOHANN WOLFGANG VON GOETHE UNIVERSITÄT

Abstract

Fachbereich 13
Institut für theoretische Physik

Bachelor Thesis

Determining the order of the phase transition in a Polyakov-loop model

by Felix MÖLLER

The kurtosis of the order parameter from a Polyakov-loop model was considered to estimate the critical point of said model at zero chemical potential μ. A linear fit near the critical point was used. Additionally, different nonlinear fit ansätze were tested on a data set containing points further away from the critical point. The validity of this method was discussed. The results from the linear fit agree with the results from previously performed simulations. Some of the nonlinear fit ansätze also proved to be successful.

Contents

Chapter 1

Introduction

The phase diagram of a statistical system describes the macroscopic behaviour of the said system, based on the value of its parameters. It is separated into different regions corresponding to different phases. When the parameters of the system change, it can undergo a transition from one phase to another, a so called phase transition. Phase transitions can be categorized into first and second order phase transitions which both exhibit characteristic behaviour. When determining the phase diagram of a system it is important to which type of phase transition is present when crossing between different regions of the phase diagram. An important feature of a phase diagram is the so **critical point**. Oftentimes, two phases are separated by a boundary line in the phase diagram. When this line is crossed, a first order phase transition occurs. This line can abruptly end in the critical point after which the distinction between two different phases becomes impossible. When changing phases by moving through the critical point, a second order phase transition occurs. See 1.1 for a qualitative visualization. A change of phase can be described using what is called an or-

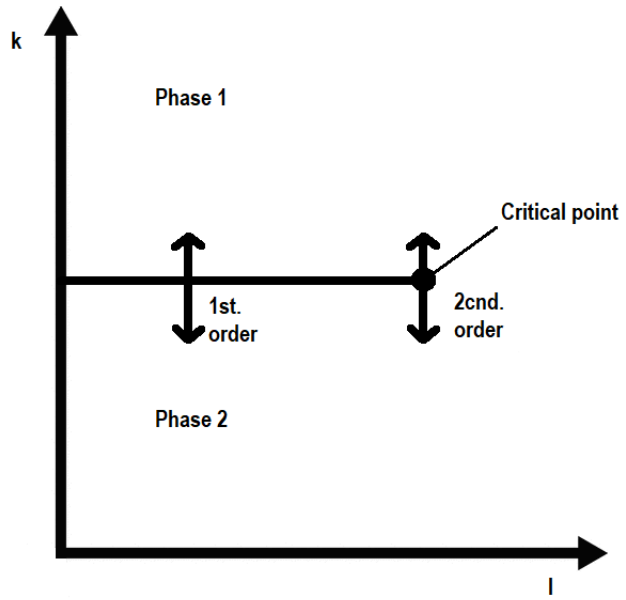

FIGURE 1.1: An exemplary phase diagram of a system with two parameters k and l. Depending on where the phase boundary is crossed, either a first or second order phase transition is observed.

der parameter. This is a parameter that has usually a value of zero in one phase and a non-zero value in the other phase, thus working as an indicator for the system's phase. Based on the current location in the phase diagram, the measurable value of the order parameter follows some probability distribution that becomes a smooth

function if the system is of finite size. By studying this distribution at the point of transition, the order of the transition can be determined. This can be achieved by inspecting the so called **kurtosis** of the distribution. It takes on different values depending on the order of phase transition at hand. When evaluating the kurtosis at multiple points on the phase boundary while in vicinity of the critical point, the kurtosis can be approximated as a linear function of the parameters of the system. Using a linear fit, the exact location of the critical point can be determined from this. This requires a set of data points for different volumes of the system that are all in direct vicinity of the critical point. Because the data points will be closely packed together, a linear fit can only give meaningful results if the error bars of the data points stay relatively small. Sometimes, high errors can arise in certain simulations, for example when dealing with quantum chromodynamics on the lattice, making the use of a linear fit inappropriate. One possible way to avoid this problem is to use data points that are further away from the critical point. The data tends to spread out for different volumes when moving away from the critical point, meaning that individual points become distinguishable even when their errors are relatively high. This has the downside that the kurtosis can not be modelled by a linear function. So far, no theoretical description of the exact function describing the kurtosis further away from the critical point is available. This thesis will try out different fit ansätze as candidates to describe the kurtosis further away from the critical point. The fits will be tried on data stemming from a certain Polyakov-loop or SU(3) spin model which was among others covered in [6]. The model can be viewed as an effective theory for quantum chromodynamics on the lattice while a comparison to the Ising model can also be drawn. The model can be simulated using a metropolis algorithm with reasonable computation time. It has the advantage that the errors produced during the simulation stay relatively small, thus even a linear fit can be performed close to the critical point and the results for nonlinear fits can be put into context. The values for the critical point will be determined from the different fits, the validity of the nonlinear fit approaches will be discussed. The estimated critical point obtained from the fitting process agrees with the results from a different simulation given in [7]. This is both true for the linear fit as well as some of the nonlinear fits that were tried out.

The thesis is structured as follows: Chapter 2 covers necessary background information about phase transitions and the Renormalization group formalism which can be used to theoretically describe certain phenomena related to phase transitions while also enabling the derivation of a general fit ansatz for the kurtosis. Chapter three will give a brief sketch of the Polyakov-loop model. Chapter four will cover the mathematical background and physical interpretation of the so called skewness and the already mentioned kurtosis. Both are quantities that describe the characteristics of a probability distribution and are essential to the analysis performed in the thesis. Chapter five will outline some numerical topics, including an outline of the metropolis algorithm, the implementation in the program ARIADNE, as well as basic information about fitting and judging the quality of a fit. Chapter six will then cover the derivation of a general fit ansatz that can be used for the kurtosis. Some possible specific ansätze are presented. Chapter seven will present the data obtained by the simulations, apply the different fit ansätze and discuss the results. Finally, chapter eight will give a brief summary about the contents and results of the thesis.

Chapter 2

Phase transitions and the Renormalization group

To start things off some general information about phase transitions and the renormalization group is presented. An introduction can be found in [3] and [2].

2.1 Phase diagrams

A phase can be understood as a certain region of space in which a system is showing homogeneous macroscopic physical properties, for example density, viscosity or magnetization. A system can typically assume more than one phase. Depending on the physical parameters of the system - temperature, pressure, etc. -, it will be in one phase or another. The different phases a system can take on can be represented in a phase-diagram which associates a set of values for the parameters of the system to the corresponding phase the system will be in at those parameters. An exemplary phase diagram is shown in figure 2.1. The parameter space is divided into different regions corresponding to the different phases. These regions are separated by boundary curves which are called phase boundaries or phase coexistence curves. At these boundaries, the system can be in two phases at once. This will be explained in more detail in the next section.

2.2 Phase Transitions

When changing the physical parameters of the system so that a phase boundary is crossed, the system will change from one phase to another, undergoing a **phase transition**. The value of a parameter at which a phase transition occurs is usually called a critical value. This is not to be confused with the **critical point** of a phase diagram. The critical point is a point in the parameter space that marks the end of a phase coexistence curve. Beyond this point, one can not distinguish between different phases anymore. To avoid confusion, in this thesis the parameter values at the critical point will be marked with the index 'cp' while the values at which a phase transition occurs will get the index 'c' as they are often called the critical values.

In order to study phase transitions, the free energy of a system has to be considered. For a canonical partition function $Z([k])$ that depends on the parameters $[k]$, the free energy $F([k])$ can be calculated using

$$F([k]) = -k_B T \ln(Z([k])) \quad . \tag{2.1}$$

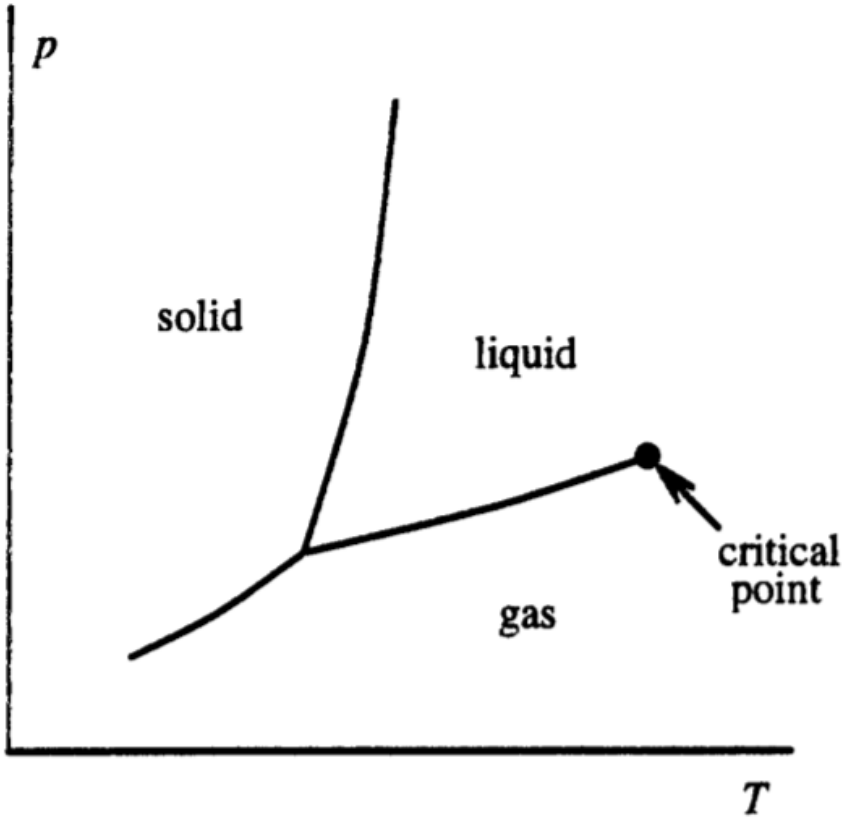

FIGURE 2.1: The phase diagram of a typical material in the p-T plane. The critical point marks the end of the liquid-gas phase coexistence curve beyond which one can't distinguish between a liquid and gaseous phase. Image taken from [2, Chapter 1.1].

A system described by a canonical partition function will try to minimize the free energy. Depending on the values of the parameters, the free energy will be minimized by the system being in one phase or another. When undergoing a phase transition, non analytical behaviour of the free energy is observed. This can fall into one of two categories, which are called first and second order phase transitions respectively. Before these categories are explained, the term **correlation length** shall be introduced. The correlation length ξ "describes the spatial extent of fluctuations in a physical quantity about the average of that quantity" [3, Ch. 2.3.3]. For example, a gas will exhibit density fluctuations in certain regions of space where the density will be near that of a liquid. The average size of these liquid like drops can be understood as the correlation length. Since the particles inside such a region are not expected to be influenced by particles out of the region, the correlation length can also be understood as the rough distance over which the behaviour of two particles in the gas correlate. With this in mind, the two types of phase transitions can be introduced:

First order or discontinuous phase transitions are characterized by a discontinuity in one of the first derivatives of $F([k])$ with respect to one the k's at $k = k_c$. At the point of transition, the correlation length is finite. Two phases coexist at once, in the sense that the total volume contains regions where the system is in one phase and regions where it is in another (in special cases, more than two phases can coexist). This is associated with discontinuous changes in physical quantities. For example the density of a material jumps in value when undergoing a first order transition from solid to liquid.

Second order or continuous phase transitions are characterized by non-analytical behaviour in one of the higher derivatives of $F([k])$ while the first derivatives all remain continuous. Non-analytical behaviour includes discontinuities but also singularities. At the point of transition the correlation diverges to infinity. This implies that the system is globally in a unique transition phase since no regional fluctuations can exist, all particles are correlated with each other. A second order phase transition occurs when passing through the critical point of the phase diagram that marks the end of a phase coexistence curve. In second order phase transitions physical quantities change continuously as they approach the critical point, as seen in figure 2.2.

Additionally, a system can also undergo a seeming change of phases without actually undergoing a phase transition as defined by the mentioned categories. This type of transition is characterized by a continuous change of the macroscopic properties of the system without encountering any non-analytical behaviour in F. The macroscopic properties of the system can differ strongly when moving a large distance in the phase diagram. Still, since no rapid some quantity at one point are observed one can not define a clear phase boundary and thus can not speak of different phases. In such a case, one speaks of **analytical crossover**. An important aspect of (theoretical) phase transitions is that they can only occur in the thermodynamic limit defined by

$$N \to \infty, \quad V \to \infty \quad , \quad \text{while} \quad \frac{N}{V} = const. \quad , \tag{2.2}$$

where N is the number of particles and V is the volume of the system. This is because the partition function is defined as either a sum or integral over *finite* quantities. Non analytical behaviour can only occur when the sum is taken over an infinite amount terms or when the integral boundaries approach infinity. Nevertheless, the study of the infinite volume limit still gives insights over physical systems. This is because a finitely sized system will always show a 'smoothed out' behaviour of the infinite volume case, i.e. a jump of some quantity in the thermodynamic limit corresponds to a rapid (but continuous) change in the finite volume case.

When describing phase transitions, introducing an **order parameter** can be useful. An order parameter is a parameter used to distinguish between two different phases. The order parameter is usually defined to be zero in one phase and non-zero in the other. For example, in a liquid-gas transition the order parameter can be defined as $\mathcal{O} = \rho_l - \rho_s$, ρ_l being the density of the liquid phase and ρ_s the current density of the system. By definition, $\mathcal{O}$ is zero when the system is in the liquid phase and non-zero when it is in the gaseous phase.

2.2.1 Scaling phenomena in second order phase transitions

One particular property of second order phase transitions is that physical quantities follow certain power laws near the critical point. In figure 2.2, we can see the magnetization as a function of the temperature for an 3D Ising ferromagnet. Near the critical temperature T_{cp} it is observed that the magnetization follows the power law

$$M \propto (T_{cp} - T)^{0.311} \quad ; \quad \text{while} \quad (T_{cp} - T) \approx 0 \quad , \quad T < T_{cp} \tag{2.3}$$

with the exponent $\beta \approx 0.311$.

Additional examples are the

$$\text{zero field susceptibility} \quad \chi = \left(\frac{\partial M}{\partial H}\right)|_{H=0} \propto \left(T - T_{cp}\right)^{-\gamma} \quad \text{where} \quad \gamma \approx 1.237,$$

$$\text{specific heat in zero field} \quad C \propto \left(T - T_{cp}\right)^{\alpha} \quad \text{where} \quad \alpha \approx 0.110 \quad .$$

The exponents arising in these power law dependencies are referred to as **critical**

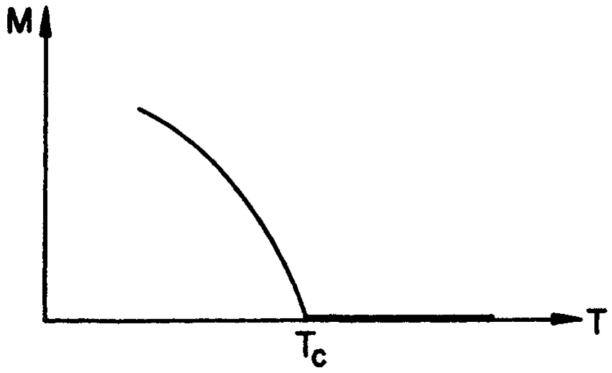

FIGURE 2.2: The magnetization as a function of the temperature in an Ising ferromagnet. The magnetization continuously decreases as one approaches T_{cp} from the left and becomes 0 from T_{cp} onwards. Near T_{cp} the magnetization follows a power law: $M \propto (T_{cp} - T)^{0.311}$. Figure from [3, section 1.2.2]

exponents. One finds that the critical exponents are not independent of each other. For example, for a d-dimensional Ising ferromagnet we have

$$\alpha = 2 - \frac{d}{y_t}$$
$$\beta = \frac{d - y_h}{y_t}$$
$$\gamma = \frac{2y_h - d}{y_t}$$

with the constants $y_t \approx 1.567$ and $y_h \approx 2.481$. The origin of these constants will become clear in section 2.3. Remarkably, the set of critical exponents is not unique to the system at hand. An identical set of exponents can be observed for two or more different systems. If two systems have the same set of critical exponents they are said to belong to the same **universality class**. Each physical system can be assigned into such a class which then determines the critical exponents. For two systems to belong to the same universality class, certain conditions have to be fulfilled:

1. The systems have to be of the same dimension
2. The symmetry group of both Hamiltonians of the systems has to coincide
3. The interaction forces are required to be of the same range (i.e. both short ranged interactions).

Besides these conditions the actual mathematical and physical details of the systems are irrelevant to the determination of the universality class.

2.3 The Renormalization Group and finite size scaling

The following discussion is based on [3, chapter 9] and [2, chapter 3].
A systematic study of scaling effects and their critical exponents as well as universality classes is given by the **Renormalization Group** formalism. For certain physical systems it is possible to describe the system with a lower number of degrees of freedom than it actually has while the large scale behaviour of the system remains unchanged. This can be achieved by a 'coarse graining' transformation, grouping together multiple degrees of freedom into a single one while changing the coupling constants determining the interaction of the different degrees of freedom. A common example for this mechanism is known as Kadanoffs block spin model:

Imagine a spin system defined on a d-dimensional cubic lattice with N lattice sites where each point is separated by the distance a. The reduced Hamiltonian $\mathcal{H}$ defined by $\mathcal{H} = \beta H$ resembles that of the Ising-model

$$\mathcal{H} = -K \sum_{<ij>} S_i S_j - h \sum_{i=1}^{N} S_i \quad . \tag{2.4}$$

Here S_i represents the spins and the couplings are given as $K = \beta J$ and $h = \beta H$ (in this case H is the magnetic field and not the Hamiltonian). The parameter β is defined as $\beta = \frac{1}{k_B T}$ and J denotes the spin coupling in the Ising-model. Since the spins are correlated on a distance of order ξ(correlation length) one can imagine dividing the system into blocks of length $a \ll la \ll \xi$ and viewing the collective behaviour of all the spins in one block as acting as a single 'block spin', see figure 2.3 . This can

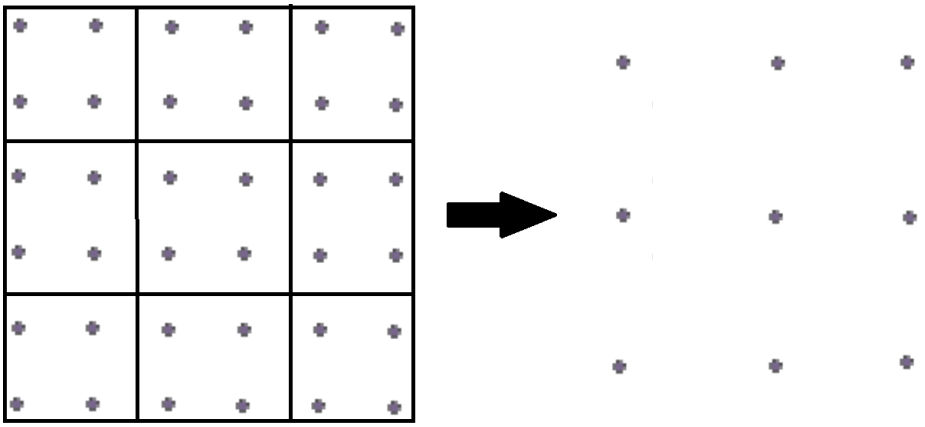

FIGURE 2.3: A 2 dimensional lattice of spins. Multiple spins can be grouped into a single block spin, thus changing the scale at that the system is viewed.

be thought of as 'zooming out' or changing the length scale at which the system is viewed. This effectively reduces the number of degrees of freedom since the system now looks like it contains less lattice sites. To account for this transformation, the couplings have to change in value while the original form of the Hamiltonian stays the same. In principle, one could repeat this transformation, again changing the value of the couplings. "Changing the length scale" of the system can be understood as changing the units under which physical quantities are expressed. For example, since the value of the lattice spacing increases after a block spin transformation and the physical value of the correlation length has to remain the same, the original correlation length ξ_0 *expressed in units of the original lattice spacing* a is smaller than the

new correlation length ξ_l *expressed in units of the new lattice spacing* la. This can be written as

$$\xi_l = l^{-1}\xi_0 \tag{2.5}$$

where ξ_0 and ξ_l are dimensionless quantities that represent the actual correlation ξ length in units of the corresponding lattice spacing. The factor l is often called the **scale factor**.

In general, a system is called *renormalizable* if a suitable coarse graining transformation can be performed. Such a transformation is then called a renormalization group (RG) transformation. The transformation is successful if the system can be described by a new Hamiltonian $\mathcal{H}'$ that has the same form as the original Hamiltonian $\mathcal{H}$ while the number of degrees of freedom is lower than before and the partition function remains unchanged. For a spin system this would mean that, if the original partition function Z is given as sum over the spins s

$$Z = \mathrm{Tr}_s\, e^{-\mathcal{H}} \quad , \tag{2.6}$$

after the transformation to the new spins s' we would have

$$Z = \mathrm{Tr}_s\, e^{-\mathcal{H}} = \mathrm{Tr}_{s'}\, e^{-\mathcal{H}'} = Z' \quad . \tag{2.7}$$

The new hamiltonian will also receive an additional term that depends only on the couplings but *not* on the degrees of freedom that are being summed over in the partition function. For example, in the blockspin model we would have

$$\mathcal{H}' = N_B \cdot g\left([k],[k']\right) + \mathcal{H}\left([k']\right) \tag{2.8}$$

with the total number of blocks N_B, some function g, the old couplings $[k]$, the new couplings $[k']$, the old hamiltonian with new couplings and new degrees of freedom $\mathcal{H}([k'])$. The additional term does not influence any expectation values since it is not affected by the sum in the partition function

$$\langle \mathcal{O} \rangle = \frac{\mathrm{Tr}'_s\, \mathcal{O} \cdot e^{-N_B \cdot g([k],[k'])+\mathcal{H}([k'])}}{\mathrm{Tr}'_s\, e^{-N_B \cdot g([k],[k'])+\mathcal{H}([k'])}} = \frac{\mathrm{Tr}'_s\, \mathcal{O} \cdot e^{-\mathcal{H}([k'])}}{\mathrm{Tr}'_s\, e^{-\mathcal{H}([k'])}} \quad , \tag{2.9}$$

thus it can be left out for such calculations. When calculating the total free energy, the additional term in the hamiltonian gives an extra contribution. For the reduced free energy $\tilde{F} = \beta F$ it can be shown that

$$\tilde{F}([k]) = -ln(Z) = N_B \cdot g([k],[k']) + l^{-d}\tilde{F}([k']) \quad . \tag{2.10}$$

In addition to the term that accounts for the change of scale $l^{-d}F([k'])$ the additional term $N_B \cdot g([k],[k'])$ represents the energy contributions of the degrees of freedom that got 'lost' during the RG transformation. Again, for any calculations deriving expectation values from the free energy this term may be ignored. In that case it is useful to define the **singular part** of the reduced free energy $\tilde{F}_s$

$$\tilde{F}_s([k]) = l^{-d}\tilde{F}([k']) \quad . \tag{2.11}$$

The term renormalization group stems from the fact that the transformations form a (semi)group, changing the length scale by a factor of l and then by a factor of l' is identical to changing it by a factor of $l + l'$ at once.

One important aspect of the RG are its **fixed points**. These are points in the

coupling space that describe a set of couplings $[K^*]$ which don't change under a RG transformation. If a RG transformation that changes the couplings from $[K]$ to $[K']$ is written as

$$[k'] = R_l([k]) \quad , \tag{2.12}$$

a fixed point in coupling space is a set of couplings $[k^*]$ that satisfy

$$[k^*] = R_l([k^*]) \quad . \tag{2.13}$$

Every point in coupling space approaches one of the fixed points under repeated RG transformations. Since a RG-transformation does *not* change the large scale behaviour of the system at hand, each fixed point corresponds to one possible phase the system can be in. Thus the phase diagram of the system can be worked out by studying the fixed points of the RG. Note that, since the correlation length transforms as

$$\xi([K']) = \frac{\xi([K])}{l} \quad , \tag{2.14}$$

at a fixed point we have

$$\xi([K*]) = \frac{\xi([K*])}{l} \quad . \tag{2.15}$$

This equation has only two solutions, $\xi = 0$ and $\xi = \infty$. The fixed point with $\xi = \infty$ corresponds to the critical point where the system is in a unique transition phase. Near a fixed point, one can describe how the couplings change under a RG transformation using simple power laws. Each coupling k is rescaled by a factor l^{y_k} where y_k is a exponent generally unique to each coupling. For example the reduced free energy density defined by $f_s = N^{-1}\tilde{F}_s$ of an Ising like system near a fixed point obeys

$$f_s(t,h) = l^{-d} f_s(t_l, h_l) = l^{-d} f_s(l^{y_t} t, l^{y_h} h) \tag{2.16}$$

for a RG transformation with scale factor l and the exponents y_t and y_h introduced in the previous section. We see that the couplings are simply rescaled by a factor of l^{y_t} and l^{y_h} respectively.

While the above presentation assumed a system of infinite size, the renormalization group framework in principle does not prohibit a finitely sized system as it simply changes the scale at which the system is viewed locally. The system size is expected to influence the behaviour of the system so it can be treated as an additional parameter for the free energy. Assuming a square system of size L^3, the singular part of the reduced free energy density can then be written as

$$f_s(t,h,L^{-1}) = l^{-d} f_s(l^{y_t} t, l^{y_h} h, lL^{-1}) \quad . \tag{2.17}$$

The scaling of $L^{-1} \rightarrow lL^{-1}$ simply comes from the fact that the length scale is changed so $L \rightarrow \frac{L}{l}$. Now in order to reach the critical point where a phase transition occurs, L has to become infinite. It is important to note that again L is an dimensionless quantity. The rescaling factor l in equation 2.17 can be set to an arbitrary value. When setting $l = L$ we get

$$f_s(t,h,L^{-1}) = L^{-d} f_s(tL^{y_t}, hL^{y_h}, 1) \tag{2.18}$$

which is equivalent to

$$L^d f_s(t,h,L^{-1}) = 1^d \cdot f_s(tL^{y_t}, hL^{y_h}, 1) \quad . \tag{2.19}$$

Since the reduced free energy density and the reduced free energy are related by $L^d f(t,h,L) = F(t,h,L)$ it follows for the singular part of the reduced free energy that

$$\tilde{F}_s(t,h,L^{-1}) = \tilde{F}_s(tL^{y_t}, hL^{y_h}, 1) \quad . \tag{2.20}$$

When dealing with finitely sized system, scaling relations such as 2.20 are often coined with the term **finite size scaling**. Equation 2.20 is an important result that will be used later.

Chapter 3

The Polyakov-loop model

The model is described by the action

$$S = -\sum_x (\sum_{k=1}^{3} \tau[L(x)L^*(x+\hat{k}) + L^*(x)L(x+\hat{k})] + \kappa[e^{\mu}L(x) + e^{-\mu}L^*(x)]) \quad . \tag{3.1}$$

The action is defined on a three-dimensional cubic lattice with sites x and the unit vectors $\hat{k}$ that are being summed over. The degrees of freedom are the fields $L(x) = \mathrm{Tr}\, W(x)$ which are calculated by taking the trace over the $SU(3)$ matrices $W(x)$. The action depends on the three parameters κ, τ, μ. The model can be viewed as an effective theory for quantum chromodynamics on the lattice [6]. In this context, the parameter τ is related to the temperature and gauge coupling, κ is related to the quark mass while μ represents the chemical potential. The traces $\mathrm{Tr}\, W(x)$ can be viewed as traces over so called *Polyakov-loops*, a term from lattice QCD, hence the name of the model. In this thesis, only the case $\mu = 0$ is considered.

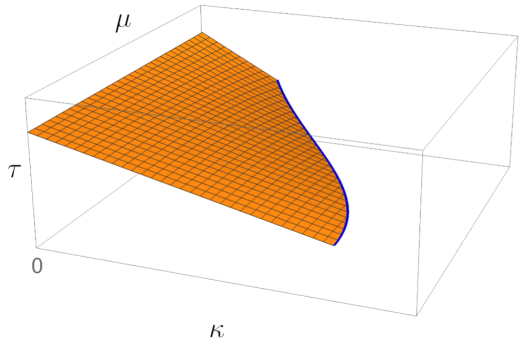

FIGURE 3.1: A schematic phase diagram for the model. The orange surface represents a phase-coexistence plane between an ordered and unordererd phase. It ends in the purple critical line at which the transition is of second order. Beyond that, analytical crossover is observed. Image taken from [6]

.

The model can also be seen as some kind of spin model. This can be seen when defining

$$\eta = \kappa e^{\mu} \quad ; \quad \bar{\eta} = \kappa e^{-\mu} \quad . \tag{3.2}$$

In this case the model exhibits a symmetry in the fields $L(x)$ when $\eta = \bar{\eta} = 0$

$$L'(x) = zL(x), \quad z \in Z(3) = \{1, e^{i\frac{\pi}{3}}, e^{i\frac{2\pi}{3}}\} \quad , \tag{3.3}$$

$Z(3)$ being the cyclic group of order 3. When $\eta, \bar{\eta} \neq 0$, this symmetry is broken. This is analogous to the Ising model where the Hamiltonian exhibits a symmetry in the

spins that is broken when the magnetic field is turned on. The expectation value $\langle L \rangle$ can then be seen as an analogy to the magnetization $M = \langle S \rangle$ in the Ising model while also acting as the order parameter.

The partition function is given as a path integral

$$Z = \int DW e^{-S[W]} \tag{3.4}$$

with the path integral measure DW, the free energy is given as $F = -\frac{1}{\beta} ln(Z)$. A schematic phase diagram for the model is given in figure 3.1. A phase coexistence plane separates an ordered and unordered phase of the system. Crossing this plane results in a first order phase transition. The plane ends in a critical line where the transition is of second order. Beyond that, analytical crossover is observed. Note again that in this thesis only the plane with $\mu = 0$ is considered.

Near the critical line the model can be described through the Ising-Model. This is why the second order phase transition transition at the critical line belongs to the same universality class as the 3D-Ising Model. Simulations have estimated the critical endpoint for $\mu = 0$ to be located at $\kappa_{cp} = 0.016 \pm 0.02$ and $\tau_{cp} = 0.1331 \pm 0.0001$ [7].

Chapter 4

The skewness and kurtosis as means to analyze phase transitions

4.1 Moments and central moments

For a random variable X with a given probability distribution $P(X)$ the so called *moments* of the probability distribution are defined as

$$m_n = \sum_x x^n \cdot P(x) \tag{4.1}$$

in the discrete case and in the continuous case as

$$m_n = \int dx \cdot x^n P(x) \quad . \tag{4.2}$$

Note that every discrete probability distribution can also be represented by a continuous distribution by using delta-distributions, from now on a continues distribution is assumed for a general description. By definition, the moments give the expectation values $\langle x^n \rangle$ of the functions $f(x) = x^n$ and contain information about the distribution. For example, the zeroth moment m_0 is just the expectation value of the distribution, the second moment is related to the variance of the distribution. One characteristic of the moments is that higher moments generally are not invariant of a shift of the distribution by a constant c. To achieve a description that only depends on the shape and not the 'location' of the distribution, one can use the *central moments* μ_n. These are defined as the expectation values of the function $f(x) = (x - \langle x \rangle)^n$ where $\langle x \rangle$ is the expectation value of x. By definition, the central moments are invariant to a shift of the distribution by some constant. The second central moment gives the variance σ^2 of the distribution, the third and fourth central moments are used to define the so called *skewness* B_3 and *kurtosis* B_4:

$$B_3 = \frac{\mu_3}{\sigma^3} \quad ; B_4 = \frac{\mu_4}{\sigma^4} \quad . \tag{4.3}$$

The skewness and kurtosis are special cases of the so called *standardized moments*

$$B_n = \frac{\mu_n}{\sigma^n} \quad . \tag{4.4}$$

Before explaining the interpretation and physical relevance of the skewness and kurtosis, more information about the calculation of these quantities is given.

4.2 Generating functions and cumulants

Consider the function $M(t)$ defined by

$$M(t) = \int_{-\infty}^{\infty} dx \cdot e^{tx} P(x) \quad . \tag{4.5}$$

By definition, the moments can be calculated from $M(t)$ using

$$m_n = \frac{d^n}{dt^n} M(t)|_{t=0} \quad . \tag{4.6}$$

Because of this property, $M(x)$ is called a *generating function* of the moments. Next to the moments one can also define the *cumulants* of a distribution. The cumulants κ_n of a distribution are similar to the moments as they as well give information about the distribution. Depending on the problem at hand, either moments or cumulants prove to be of better use. The cumulants can be defined using their generator function $K(x)$, which is in turn defined as the logarithm of the moment generating function

$$K(t) = \ln(M(t)) \quad . \tag{4.7}$$

The n-th cumulant κ_n is then given as

$$\kappa_n = \frac{d^n}{dt^n} K(t)|_{t=0} \quad . \tag{4.8}$$

The first two cumulants are the expectation value and the variance of the distribution respectively. The cumulants can be expressed using moments, for example for the first four cumulants we have

$$\begin{aligned}
\kappa_1 &= m_1 \\
\kappa_2 &= m_2 - m_1^2 \\
\kappa_3 &= m_3 - 3m_2m_1 + 2m_1^3 \\
\kappa_4 &= m_4 - 4m_3m_1 - 3m_2^2 + 12m_2m_1^2 - 6m_1^4
\end{aligned}$$

Using these relations it can be shown that the skewness and kurtosis can be calculated via

$$B_3 = \frac{\kappa_3}{\kappa_2^{3/2}} \quad ; \quad B_4 = \frac{\kappa_4}{\kappa_2^2} + 3 \quad . \tag{4.9}$$

These relations allow the calculation of the skewness and kurtosis of a distribution via the free energy F of a system. This is because the partition function Z serves (up to a factor) as the cumulant generating function. The cumulants of the distribution of the internal energy U of a system can be calculated by using

$$\kappa_n = (-1)^k \frac{\partial^n}{\partial \beta^n} Z(\beta) \quad . \tag{4.10}$$

Depending on the variables in whose respect is being differentiated to, the cumulants for different distributions is obtained. For example in an Ising like system, differentiating with respect to h gives the cumulants for the distribution of the magnetization M. Since the partition function and the free energy are related by

$$F = -k_B T \ln(Z) = -\frac{1}{\beta} \ln(Z) \quad . \tag{4.11}$$

the cumulants can be calculated using

$$\kappa_n = (-1)^{k+1} \frac{\partial^k}{\partial \alpha^k} \beta F \tag{4.12}$$

with some general parameter in whose respect is being differentiated to. Additionally, since the cumulants can be related to the moments - which are in turn defined as expectation values - it is sufficient to use the singular part of the free energy when applying equation 4.12.

4.3 Interpretation of the skewness

The skewness of an observable gives information about the asymmetry of the related distribution around its mean. Three different distributions with varying skewness are shown in figure 4.1. One distribution is perfectly symmetrical (coloured in blue), which corresponds to a skewness equal to 0. The other two distributions (coloured in red and green) exhibit clear asymmetry. This is represented by either a positive skewness for the green distribution or a negative skewness for the red distribution.

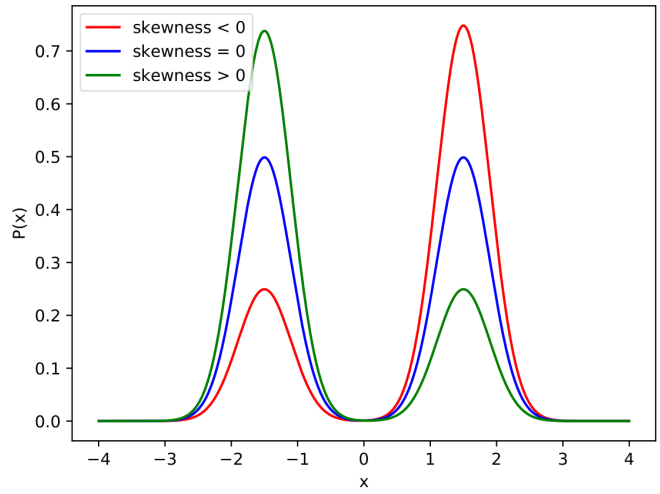

FIGURE 4.1: Three exemplary (non-normalized) distributions P(x) that exhibit either positive, negative and zero skewness.

In a physical context, the skewness can be used to determine the critical values at which a phase transition occurs. In an infinitely sized system, the distribution of the order parameter will be represented by a delta-distribution either centered at $\beta_0 = 0$ for one phase or at a non-zero value β_1 for the other phase. This is different for a finitely sized system, where a true phase transition cannot be observed. When in a certain region of the phase diagram corresponding to one phase, the distribution of the order parameter will still have a non-zero chance for the order parameter to assume a value corresponding to a different phase. This corresponds to a fact that a true phase transition cannot occur in finitely sized systems. The distribution will have *two* peaks, one around zero for one phase and one around the non-zero value for the other phase, similar to the distributions shown in figure 4.1. Depending on how far away the system is from the (theoretical) point of phase transition, one peak will be considerably larger. When crossing between the regions corresponding to

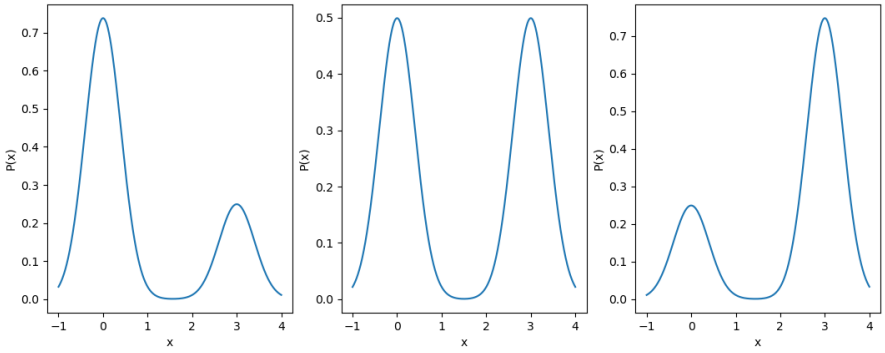

FIGURE 4.2: The distribution of the order parameter P(x) changes as the variable x is varied. At the point of transition the distribution becomes symmetric which is represented by the middle graph.

the two phases, at one point both peaks have to be of equal size, meaning that the distribution is symmetric. This point can then be interpreted as the point of phase transition. In figure 4.2 this phenomenon is qualitatively portrayed.

Note that this argument does not depend on the type of phase transition as the only criterion is the symmetry of the distribution at the point of transition and not the actual type or shape of it. It can be used to determine the point of first order phase transition or the critical point for the second order phase transition, although it will give no direct information about the order at hand. Even when dealing with an analytical crossover, some kind of 'transition point' can be assigned using this method.

4.4 Interpretation of the kurtosis

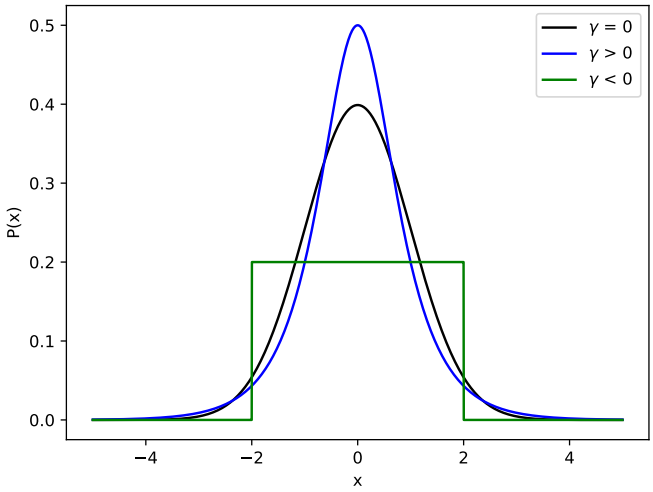

FIGURE 4.3: Three exemplary (non normalized) distributions P(x) with varying excess kurtosis γ.

The kurtosis of an observable gives information about the 'tailedness' of the distribution, i.e. the thickness of the distributions tail. The kurtosis of a distribution is

often expressed using the so called *excess kurtosis* γ which is defined by subtracting 3 from the kurtosis

$$\gamma = B_4 - 3 \quad . \tag{4.13}$$

This relates the kurtosis of a distribution to the kurtosis of the normal distribution, which is equal to three. If a distribution has a tail that is thicker than that of the normal distribution, the excess will be greater than zero and vice versa. In figure 4.3 this is shown for three exemplary distributions, one of them being a normal distribution. The excess kurtosis is the derivative of the skewness.

In general, two distributions of different shapes are expected to have different kurtosis values. This is why the kurtosis can be used to determine the order of a phase transition: Depending on the order of phase transition, the distribution of the order parameter has a different shape and hence a different kurtosis value. See table 4.1 for a comparison of the possible kurtosis values. For a first order phase transition, the distribution is the sum of two normal distributions which results in a kurtosis $B_4 = 1$. For a crossover transition, the distributions is a normal distribution with a kurtosis value $B_4 = 3$. For a second order phase transition where the system is in a unique transition phase, the shape of the distribution is non trivial and the kurtosis cannot be calculated directly. It has to be determined numerically or experimentally and is unique to the universality class at hand. For the Polyakov-loop model belonging to the 3D-Ising universality class, the kurtosis takes the value of $B_4(CP) = 1.604$ at the critical point. As the excess kurtosis is the derivative of the skewness, the kurtosis is expected to be a local extremum when the skewness is equal to 0. For a fixed value of κ and varying τ near τ_c, the skewness and excess kurtosis show a behaviour similar to that pictured in figure 4.4 while the point at which the skewness is equal to 0 and the excess kurtosis is minimized corresponds to τ_c.

Type of transition:	1st. order	2nd. order	crossover
Kurtosis:	1	1.604	3

TABLE 4.1: The different kurtosis values for the distribution of the order parameter, depending on the type of transition.

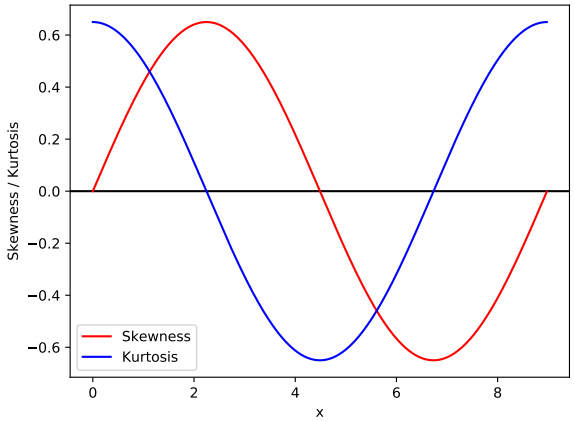

FIGURE 4.4: The expected qualitative behaviour of the skewness and kurtosis when varying τ near τ_c while κ is fixed.

Chapter 5

Numerical aspects

5.1 The Metropolis algorithm

The Metropolis algorithm is a way to numerically approximate the expectation value of an observable $\langle \mathcal{O} \rangle$ in many particle systems. It is a special case of what is called a *Monte-Carlo* algorithm. A brief presentation following chapter 4 of [1] will be given here.

5.1.1 Monte-Carlo importance sampling

The basic idea of a Monte-Carlo algorithm is numerically approximating some unknown quantity by summing over a large amount of samples. For example, the expectation value of a function $f(x)$ weighted by a probability distribution $\rho(x)$

$$\langle f \rangle = \frac{\int dx \rho(x) f(x)}{\int dx \rho(x)} \tag{5.1}$$

can be written as

$$\langle f \rangle = \lim_{N \to \infty} \frac{1}{N} \sum_{n}^{N} f(x_n) \tag{5.2}$$

when the N samples x_n are taken so that they follow the probability distribution $\rho(x)$. While an infinite amount of samples gives an exact value, using a finite amount leads only to an approximation. In a statistical system governed by a partition function Z given as a path integral

$$Z = \int D[W] e^{-S[w]} \tag{5.3}$$

the expectation value of an observable $\langle \mathcal{A} \rangle$ can be calculated with

$$\langle \mathcal{A} \rangle = \frac{\int D[W] e^{-S[w]} \mathcal{A}[W]}{Z} \quad . \tag{5.4}$$

Here W represents the degrees of freedom that are being integrated over. This has the same mathematical structure as the expectation value of a random function $f(x)$ weighted by a probability distribution $\rho(x)$, taken that the Boltzmann-factor $e^{-S[W]}$ is interpreted as the probability distribution ρ. This means that expectation values calculated from a path integral can be numerically approximated by taking samples according to the probability distribution and using equation 5.2. The statistical error

when approximating $\langle \mathcal{A} \rangle$ using N samples W_n is of order $\mathcal{O}(\frac{1}{\sqrt{N}})$. We have

$$\langle \mathcal{A} \rangle = \frac{1}{N} \sum_{n}^{N} \mathcal{A}[W_n] + \mathcal{O}(\frac{1}{\sqrt{N}}) \quad . \tag{5.5}$$

As the samples are taken according to their 'importance' given by the probability distribution $e^{-S[W]}$, this method of calculating expectation values is called Monte-Carlo importance sampling.

5.1.2 Markov-Chains and the Metropolis algorithm

A potential method to take the samples W_n according to the distribution $e^{-S[W]}$ is the construction of a so called *Markov-Chain*. The general idea is to construct a stochastic sequence of field/variable configurations $\{W_n\}$ that follow the distribution. The sequence randomly transitions between different configurations while every transition from one configuration to another is assigned a certain probability. By carefully constructing a set of rules that define the transition probabilities, a sequence of configurations following the probability distribution can be achieved. There is no unique way to construct such a set of rules. A possible method is the Metropolis algorithm. One iteration in the Markov-chain works as follows:

1. Starting from the configuration W_n, randomly select another configuration W_{n+1} with the selection probability $T_S(W_{n+1}|W_n)$ (read as: The probability to select the configuration W_{n+1} when starting from W_n) that is defined for all pairs of W_n and W_{n+1}.

2. The new configuration is accepted as the next configuration in the Markov-chain with an acceptance probability of

$$T_A(W_{n+1}|W_n) = \min(1, \frac{T_S(W_n|W_{n+1})e^{-S[W_{n+1}]}}{T_S(W_{n+1}|W_n)e^{-S[W_n]}}) \quad . \tag{5.6}$$

   This is defined so that the new configuration is guaranteed to be accepted if $T(W_n|W_{n+1})e^{-S[W_{n+1}]} \geq T(W_{n+1}|W_n)e^{-S[W_n]}$. On the other hand, if $T(W_n|W_{n+1})e^{-S[W_{n+1}]} < T(W_{n+1}|W_n)e^{-S[W_n]}$, the new configuration is accepted with a probability equal to $\frac{T(W_n|W_{n+1})e^{-S[W_{n+1}]}}{T(W_{n+1}|W_n)e^{-S[W_n]}}$). If the selection probability $T_S(W_{n+1}|W_n)$ is defined so that $T_S(W_{n+1}|W_n) = T_S(W_n|_{n+1})$, the acceptance probability reduces to

$$T_A(W_{n+1}|W_n) = \min(1, \frac{e^{-S[W_{n+1}]}}{e^{-S[W_n]}}) \quad . \tag{5.7}$$

   For this case, the new configuration is guaranteed to be accepted if it is more likely to occur according to the Boltzmann-factor $e^{-S[W]}$.

3. If the configuration was accepted, repeat step 1 with the new configuration as the starting point. If it was rejected, the old configuration is used again. Proceeding one step in the Markov-chain is called an *update*.

By construction of the algorithm, configurations that are more likely according to the Boltzmann-factor will be visited more often in the Markov-chain than configurations occurring less likely. It can be shown that the sample distribution of this algorithm eventually resembles the distribution given by the Boltzmann factor. Some reasonable amounts of updates have to be done so the desired distribution is resembled.

The Metropolis algorithm for the Polyakov-loop model

The application of the Metropolis algorithm for the Polyakov-loop model is done in the program ARIADNE by Wolfgang Unger. Some further considerations have to be taken when practically applying the algorithm here. The model is defined on a cubic lattice with N_s^3 lattice sites. The possible configurations of the system depend on the matrices $W(x)$ which form the fields $L(x)$. Instead of completely changing the systems configuration by updating every lattice site at once, only one lattice site at a time is updated when proceeding in the Markov-chain. This is done by randomly selecting one lattice site to update before step 1 in the procedure described above. Otherwise the procedure is identical. Here the selection probability $T_S(W_{n+1}|W_n)$ is defined so that $T_S(W_{n+1}|W_n) = T_S(W_n|W_{n+1})$ and equation 5.7 holds. Only accepting one lattice site at a time has the consequence that measurements taken on consecutive configurations are correlated. This is because changing a single lattice site is not expected to change the value of an observable $\mathcal{A}$ by a large amount. Using only correlated measurements would lead to additional errors in the approximation for the expectation value of $\mathcal{A}$. To get reasonably uncorrelated measurements, a measurement of $\mathcal{A}$ is only taken after N_S^3 updates. Besides some other observables, the program ARIADNE takes measurements of the order parameter $\langle L \rangle$, the susceptibility (derivative) of the order parameter and the skewness and kurtosis of the order parameter $\langle L \rangle$.

5.2 The jackknife method

The jackknife method is a method that can be used to estimate the variance of some function $f(x)$ depending on a statistical parameter x. It is explained in detail in [9], some central results will be presented in this section.

Suppose we have a sample of N data points for the random variable x. Then the i-th jackknife average x_i^J for this sample is defined by averaging over the whole sample except the i-th point

$$x_i^J = \sum_{n \neq i} \frac{x_n}{N-1} \quad . \tag{5.8}$$

Consequently, the i-th jackknife average of a function f_i^J is defined by taking the jackknife average for x as argument

$$f_i^J = f(x_i^J) \quad . \tag{5.9}$$

Then the jackknife estimate for $f(\langle x \rangle)$, $\langle x \rangle$ being the true average (or expectation value) of x, is given as average over all jackknife averages

$$\bar{f}^J = \sum_{i=1}^{N} \frac{f_i^J}{N} \quad . \tag{5.10}$$

The variance of the jackknife averages $\sigma_{f_J}^2$ is defined as

$$\sigma_{f_J}^2 = \overline{(f_J)^2} - (\bar{f}_J)^2 \tag{5.11}$$

where $\overline{(f_J)^2}$ is defined as

$$\overline{(f_J)^2} = \sum_{i=1}^{N} \frac{(f_i^J)^2}{N} \quad . \tag{5.12}$$

It can be shown that the true variance σ_f^2 of $f(\langle x \rangle)$ can be estimated using the jackknife variance with

$$\sigma_f^2 = \sigma_{f_J}^2 \sqrt{N-1} \quad . \tag{5.13}$$

Note that this method can also be generalized for functions that depend on more than one random variable. The program ARIADNE uses the jackknife method to estimate the errors for the skewness and kurtosis.

5.3 Basics of fitting

In this section some basic concepts about fitting a function to a given set of data points is presented. As in the previous section, a detailed discussion can be found in [9]. Suppose we have a set of N data points (x_i^d, y_i^d) and want to model this data using a function $f(x)$. The basic idea of fitting is finding the values for a set of M fit parameters defining the function $f(x)$ so that the function models the data in a satisfying way. While 'satisfying' is an ambiguous criterion, the most common way to achieve a good fit is to minimize a quantity known as chi-squared. This is defined as

$$\chi^2 = \sum_{i=1}^{N} \left(\frac{y_i^d - f(x_i)}{\sigma_i} \right)^2 \tag{5.14}$$

where σ_i is the error for $f(x_i)$. This quantity represents the sum of the squared deviations of the data points from the fitting function while each deviation is weighted by the corresponding error. The error weight ensures that data points with large errors contribute less to the overall sum. To judge the quality of a fit achieved by minimizing chi-squared, additional quantities have to be considered. One of those quantities is chi-squared per degrees of freedom $\chi^2_{N_{DOF}}$, defined as

$$\chi^2_{DOF} = \frac{\chi^2}{N_{DOF}} \tag{5.15}$$

with the number of degrees of freedom N_{DOF}. The number of degrees of freedom is the amount of independent fitting parameters. In general the fitting parameters are related to the data points, the knowledge of N_{DOF} parameters automatically defines the others. With N data points and M fitting parameters, the number of degrees of freedom is

$$N_{DOF} = N - M \quad . \tag{5.16}$$

A good fit should assume a value of $\frac{\chi^2}{N_{DOF}} \approx 1$. This can qualitatively understood if assuming that all data points have the same average error σ_{avg} so that

$$\chi^2_{DOF} = \sum_{i=1}^{N} \left(\frac{y_i^d - f(x_i)}{N_{DOF} \cdot \sigma} \right)^2 \quad . \tag{5.17}$$

Having $\frac{\chi^2}{N_{DOF}} = 1$ would mean that the sum of all deviations is equal to N_{DOF} times the average error. A value less than 1 would mean that the sum of the deviations is *less* than the average error times N_{DOF}, meaning that the fit models the data better than it should be possible according to the errors. This phenomenon is also called 'overfitting'. On the other hand, a value greater than 1 would mean that the fit does not model the data as good as potentially possible when accounting for the errors.

Another quantity to judge the quality of the fit is the parameter Q defined as

$$Q = \frac{1}{\Gamma\left(\frac{N_{DOF}}{2}\right)} \int_{\frac{\chi^2}{2}}^{\infty} dy \cdot y^{\frac{N_{DOF}}{2}-1} e^{-y} \tag{5.18}$$

with the Euler gamma function $\Gamma(x)$. The interpretation of Q can be explained as follows: Every data sample comes with errors for every point. The size of the errors follows a probability distribution that can be assumed to be Gaussian. The parameter Q gives the probability that the given fit would lead to a value of χ^2 equal or higher than the original χ^2 if one would apply the fit to a different data sample (where the errors follow the same probability distribution). A probability close to 1 would mean that most other possible data samples likely had a higher value of χ^2. This is another hint at overfitting, the fit being better than it should be possible. A probability close to 0 would mean that it is very likely that other data sets would result in a lower value for χ^2, indicating that the fit is not good enough and . A good fit should assume an in between value of $Q \approx 0.5$.

Chapter 6

Fit ansätze for the kurtosis

6.1 Finite size scaling analysis for the kurtosis

This section will develop a general fit ansatz for the kurtosis. Recall equation 4.9 relating the kurtosis to the cumulants

$$B_4 = \frac{\kappa_4}{\kappa_2^2} + 3 \tag{6.1}$$

as well as equation 4.12 which allows to calculate the cumulants using the free energy

$$\kappa_n = (-1)^{k+1} \frac{\partial^k}{\partial \alpha^k} \beta F = (-1)^k \frac{\partial^k}{\partial \alpha^k} \widetilde{F}$$

with the reduced free energy $\widetilde{F}$. Combining these relations leads to

$$B_4 = \frac{\frac{\partial^4}{\partial \alpha^4} \widetilde{F}}{(\frac{\partial^2}{\partial \alpha^2} \widetilde{F})^2} + 3 \tag{6.2}$$

Instead of doing this calculation for the free energy of the Polyakov-loop model it is done for a free energy of an Ising-like system with variables t and h. This is because the exponents y_t and y_h are known for the Ising model which can be used in the derivation. Near the critical point one can map the arguments t and h of the Ising model to the arguments τ and κ of the Polyakov-loop model. This can be explained using universality, since both models belong to the same universality class they exhibit similar scaling behaviour near the critical point. There the parameters of both models can be related via linear combinations [5]

$$\begin{aligned} t &= A(\tau - \tau_{cp}) + B(\kappa - \kappa_{cp}) \\ h &= C(\tau - \tau_{cp}) + D(\kappa - \kappa_{cp}) \end{aligned} \tag{6.3}$$

with A, B, C, D being constants. Recall that, depending on the variable in whose respect the derivatives in 6.2 are being taken to, the kurtosis of a different observable is obtained. The derivative corresponding to the kurtosis of a general observable in an Ising like system can be written as a linear combination of an energy-like and magnetic-like part [8]

$$\frac{\partial}{\partial \alpha} = c_E \frac{\partial}{\partial t} + c_M \frac{\partial}{\partial h} \tag{6.4}$$

with c_E and c_M being constants. Now recall relation 2.20 derived in chapter 2.3 and set $L = N_s$, N_s being the number of lattice sites contained in one edge of a three dimensional cube,

$$\tilde{F}_s(t, h, N_s^{-1}) = \tilde{F}_s(tN_s^{y_t}, hN_s^{y_h}, 1) \quad . \tag{6.5}$$

This leads to

$$B_4 = \frac{\frac{\partial^4}{\partial\alpha^4}\widetilde{F}\left(t,h,N_s^{-1}\right)}{\left(\frac{\partial^2}{\partial\alpha^2}\widetilde{F}(t,h,N_s^{-1})\right)^2} + 3 = \frac{\left(c_E\frac{\partial}{\partial t} + c_M\frac{\partial}{\partial h}\right)^4 \tilde{F}\left(tN_s^{y_t}, hN_s^{y_h}, 1\right)}{\left[\left(c_E\frac{\partial}{\partial t} + c_M\frac{\partial}{\partial h}\right)^2 \tilde{F}\left(tN_s^{y_t}, hN_s^{y_h}, 1\right)\right]^2} + 3 \tag{6.6}$$

The fraction has to be further evaluated. For convenience the following notation will be used

$$\frac{\partial^k}{\partial\alpha^k} = \partial\alpha^k \quad ; \quad \partial t^m \partial h^n \tilde{F}\left(tN_s^{y_t}, hN_s^{y_h}, 1\right) = \tilde{F}^{mn} \quad . \tag{6.7}$$

The numerator evaluates to

$$\begin{aligned}\kappa_4 &= \left(c_E^4\partial t^4 + 4c_E^3\partial t^3 c_M\partial h + 6c_M^2c_E^2\partial t^2\partial h^2 + 4c_e c_M^3\partial t\partial h^3 + c_M^4\partial h^4\right)\tilde{F}^{00} \\ &= c_E^4\tilde{F}^{40}N_s^{4y_t} + 4c_E^3c_M\tilde{F}^{31}N_s^{3y_t}N_s^{y_h} + 6c_M^2c_E^2\tilde{F}^{22}N_s^{2y_t}N_s^{2y_h} + 4c_Mc_E^3\tilde{F}^{13}N_s^{y_t}N_s^{3y_h} \\ &\quad + c_M^4\tilde{F}^{04}N_s^{4y_h} \quad .\end{aligned} \tag{6.8}$$

Now $c_M^4\tilde{F}^{40}N_s^{4y_h}$ can be factored out, leading to

$$\begin{aligned}\kappa_4 = c_M^4\tilde{F}^{04}N_s^{4y_h}\Bigg(&\frac{c_E^4\tilde{F}^{40}}{c_M^4}\,\tilde{F}^{04}N_s^{4y_t-4y_h} + \frac{4c_E^3\tilde{F}^{31}}{c_M^3\tilde{F}^{04}}N_s^{3y_t-3y_h} + \frac{6c_E^2\tilde{F}^{22}}{c_M^2\tilde{F}^{04}}N_s^{2y_t-2y_h} \\ &+ \frac{4c_E^3\tilde{F}^{13}}{c_m^3\tilde{F}^{04}}N_s^{y_t-y_h} + 1\Bigg) \quad .\end{aligned} \tag{6.9}$$

The term in the bracket can now be approximated to only include the contributions of greatest order. Since $y_h > y_t$ and $y_t - y_h \approx -0.9$, every factor of the form $N_s^{ny_h-ny_t}$ results in a suppression of the associated term with a factor of $N_s^{-0.9}$ compared to the term with the factor $N_s^{(n-1)y_t-(n-1)y_h}$ (see table 6.1). This is why the expression can be approximated as

$$\kappa_4 = c_M^4\tilde{F}^{04}N_s^{4y_h}\left[1 + \frac{4c_E^3\tilde{F}^{13}}{c_m^3\tilde{F}^{04}}N_s^{y_t-y_h} + \mathcal{O}\left(N_s^{2y_t-2y_h}\right)\right] \quad . \tag{6.10}$$

$y_t - y_h$	-0.8948
$2y_t - 2y_h$	-1.7896
$3y_t - 3y_h$	-2.6844
$4y_t - 4y_h$	-3.5792

TABLE 6.1: The values for $ny_t - ny_h$ for different n.

The denominator is evaluated in a similar fashion,

$$\begin{aligned}\kappa_2^2 &= \left[\left(c_E^2\partial t^2 + 2c_Ec_M\partial t\partial h + c_M^2\partial h^2\right)\tilde{F}^{00}\right]^2 \\ &= c_M^4\left(\tilde{F}^{20}\right)^2N_s^{2y_t} + 4c_E^3c_M\tilde{F}^{20}\tilde{F}^{11}N_s^{3y_t}N_s^{y_h} + 2c_E^2c_M^2\tilde{F}^{20}\tilde{F}^{02}N_s^{2_t}N_s^{2y_h} \\ &\quad + 4c_Ec_M^3\tilde{F}^{11}\tilde{F}^{02}N_s^{y_t}N_s^{3y_h} + 4c_E^2c_M^2\left(\tilde{F}^{11}\right)^2N_s^{2y_t}N_s^{2y_h} + c_M^4\left(\tilde{F}^{02}\right)^2N_s^{4y_h} \\ &= c_M^4\left(\tilde{F}^{02}\right)^2N_s^{4y_h}\left[1 + \frac{4c_E\tilde{F}^{11}}{c_M\tilde{F}^{02}}N_s^{y_t-y_h} + \mathcal{O}\left(N_s^{2y_t-2y_h}\right)\right] \quad .\end{aligned} \tag{6.11}$$

Now the kurtosis evaluates to

$$B_4 = \frac{\tilde{F}^{04}}{\left(\tilde{F}^{02}\right)^2} \frac{\left[1 + \frac{4c_E^3 \tilde{F}^{13}}{c_m^3 \tilde{F}^{04}} N_s^{y_t - y_h} + \mathcal{O}\left(N_s^{2y_t - 2y_h}\right)\right]}{\left[1 + \frac{4c_E \tilde{F}^{11}}{c_M \tilde{F}^{02}} N_s^{y_t - y_h} + \mathcal{O}\left(N_s^{2y_t - 2y_h}\right)\right]} + 3 \quad . \tag{6.12}$$

A fraction of the form $\frac{1+x}{1+y}$ can be approximated as $(1+x)\left(1 - y + \mathcal{O}\left(y^2\right)\right)$ if one expands around $y = 0$, leading to

$$\begin{aligned} B_4 &= \frac{\tilde{F}^{04}}{\left(\tilde{F}^{02}\right)^2} \left[1 + \frac{4c_E^3 \tilde{F}^{13}}{c_m^3 \tilde{F}^{04}} N_s^{y_t - y_h} + \mathcal{O}\left(N_s^{2y_t - 2y_h}\right)\right] \left[1 - \frac{4c_E \tilde{F}^{11}}{c_M \tilde{F}^{02}} N_s^{y_t - y_h} + \mathcal{O}\left(N_s^{2y_t - 2y_h}\right)\right] + 3 \\ &= \frac{\tilde{F}^{04}}{\left(\tilde{F}^{02}\right)^2} \left[1 + \left(\frac{4c_E^3 \tilde{F}^{13}}{c_M^3 \tilde{F}^{04}} - \frac{4c_E \tilde{F}^{11}}{c_M \tilde{F}^{02}}\right) + \mathcal{O}\left(N_s^{2y_t - 2y_h}\right)\right] + 3 \qquad (6.13) \\ &= \frac{\tilde{F}^{04}}{\left(\tilde{F}^{02}\right)^2} \left[1 + C N_s^{y_t - y_h} + \mathcal{O}\left(N_s^{2y_t - 2y_h}\right)\right] + 3 \qquad (6.14) \end{aligned}$$

where in the last step the constant $C = \left(\frac{4c_E^3 \tilde{F}^{13}}{c_M^3 \tilde{F}^{04}} - \frac{4c_E \tilde{F}^{11}}{c_M \tilde{F}^{02}}\right)$ was defined. C is only approximately a constant near the fixed point as the derivatives of $\tilde{F}$ depend on t. Equation 6.13 is exactly the result given in [8]. When dropping the terms of order $\mathcal{O}\left(N_s^{2y_t - 2y_h}\right)$ the final result is

$$B_4 = \frac{\tilde{F}^{04}\left(tN_s^{y_t}, hN_s^{y_h}, 1\right)}{\left(\tilde{F}^{02}\left(tN_s^{y_t}, hN_s^{y_h}, 1\right)\right)^2} \left(1 + C N_s^{y_t - y_h}\right) + 3 \quad . \tag{6.15}$$

Before transforming to the parameters of the Polyakov-loop model, one can set $h = 0$. This can again be explained using universality: In the Ising model the phase diagram near the critical point in the $t - h$-plane consists of a line of first order phase transition that ends in the critical point at $t = h = 0$ (see figure 6.1). When sufficiently close to the critical point, the first order transition line ending in the critical point in the Polyakov-loop model can also be assumed to be linear. In this thesis, the kurtosis is evaluated at multiple points on (and beyond) this line. The parameter κ is varied and the corresponding critical value of τ is evaluated using analysis of the skewness. Since - near the critical point - there is a correspondence between the parameters of both models, 'moving' on the first order transition line in the Polyakov-loop model corresponds to 'moving' on the first order transition line in the Ising-model. Since this line is located at $h = 0$ in the Ising-model, one can set $h = 0$ before transforming to the parameters τ and κ. Additionally, since the kurtosis is evaluated on an approximately straight line in the phase diagram of the Polyakov-loop model, the parameters τ and κ can be related via the linear equation describing the line so we can write

$$\tau - \tau_{cp} = X(\kappa - \kappa_{cp}) \tag{6.16}$$

with X being a constant. Combining this with equation 6.3 means that, on the line where the kurtosis is being evaluated, t can be transformed into κ using

$$t = Y(\kappa - \kappa_{cp}) \tag{6.17}$$

with Y again being a constant.

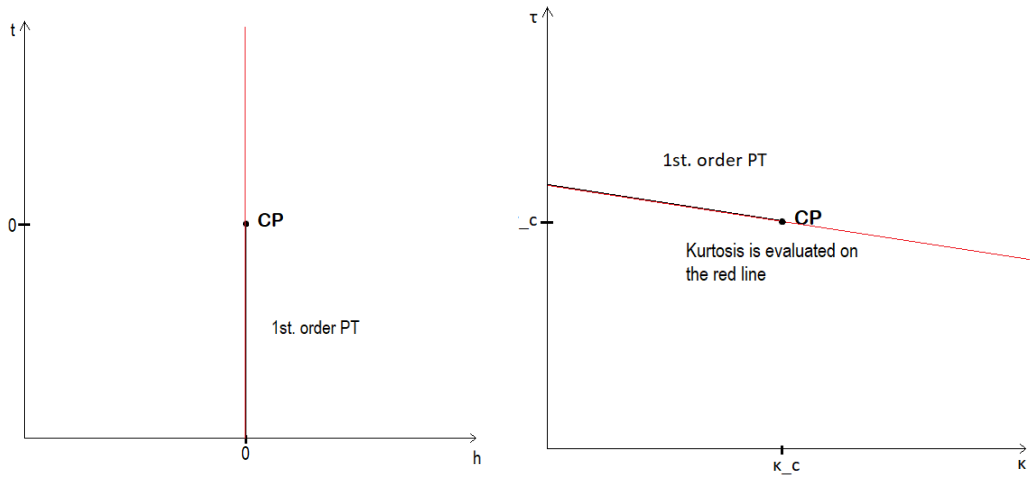

FIGURE 6.1: The schematic phase diagrams for the Ising-Model and the Polyakov-loop model near the critical point (CP). Image similar to figure 3.2 of [4].

Setting $h = 0$ the kurtosis near the critical point becomes

$$B_4 = \frac{\tilde{F}^{04}\left(tN_s^{y_t}, 0, 1\right)}{\left[\tilde{F}^{02}\left(tN_s^{y_t}, 0, 1\right)\right]^2}\left(1 + CN_s^{y_t - y_h}\right) + 3 \tag{6.18}$$

$$= G\left(tN_s^{y_t}\right)\left(1 + CN_s^{y_t - y_h}\right) \tag{6.19}$$

where the fraction in expression 6.18 was written as a function $G(tN_s^{y_t})$. The constant $+3$ can also be absorbed into the function $G\left(tN_s^{y_t}\right)$. To find a fit for the kurtosis, different functions can be tried for $G(x)$ while treating C as an additional fit parameter. To conclude this calculation it is useful to consider the kurtosis of a purely magnetization like observable. This corresponds to setting $c_E = 0$ in equation 6.4. In this case the kurtosis reduces to

$$B_4 = \frac{c_M \partial h^4 \tilde{F}\left(tN_s^{y_t}, hN_s^{y_h}, 1\right)}{\left[c_M \partial h^2 \tilde{F}\left(tN_s^{y_t}, hN_s^{y_h}, 1\right)\right]^2} + 3 \quad . \tag{6.20}$$

After setting $h = 0$ this equals

$$B_4 = \frac{\tilde{F}^{04}\left(tN_s^{y_t}, 0, 1\right)}{\left[\tilde{F}^{02}\left(tN_s^{y_t}, 0, 1\right)\right]^2} + 3 \tag{6.21}$$

$$= G\left(tN_s^{y_t}\right) \quad . \tag{6.22}$$

Note that we arrive at exactly the same result as before except the additional factor $\left(1 + CN_s^{y_t - y_h}\right)$ is missing, hence the function $G(x)$ here is identical to that in expression 6.19. At the critical point where $t = 0$, the kurtosis becomes independent of the volume. This means that a fit ansatz for $G(x)$ has to be equal to the critical kurtosis value, regardless of the volume.

6.2 Possible ansätze

Before presenting the different ansätze that will be tried in this thesis, a brief sketch of how the function $G(x)$ in equation 6.19 should behave will be given. As discussed

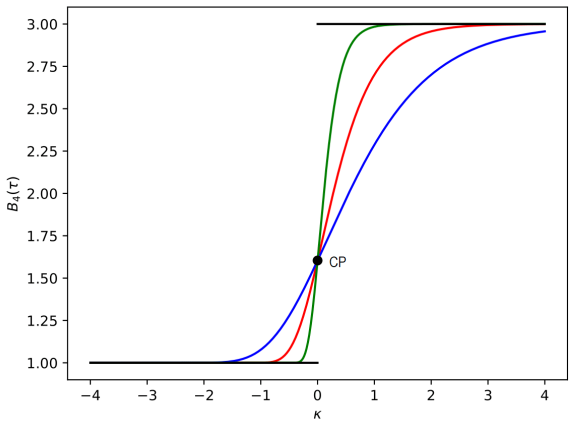

FIGURE 6.2: Schematic course of the function G(x) for different volumes modeling the kurtosis of a purely magnetic like observable. The black curve represents the infinite volume limit.

in the previous section, at the critical point the kurtosis should be independent of the volume and all curves for different volumes should cross at the corresponding kurtosis value. This can be achieved by demanding that $G(0) = B_4(CP)$. When replacing the argument $tN_s^{y_t}$ with $Y\left(\kappa - \kappa_{cp}\right) N_s^{y_t}$ according to equation 6.17, this corresponds to $\kappa = \kappa_{cp}$. Note that for all fits tried out, the constant Y in equation 6.17 can be absorbed into the fitting parameters and will be left out from now on. For the 3D-Ising universality class we have $B_4(CP) = 1.604$. In the infinite volume limit, the kurtosis takes either the value 1 or 3 corresponding to a first order transition or an analytical crossover as previously discussed in section 4.4. For a finite volume the curve should be a smoothed out version of the infinite volume limit with the asymptotic behaviour

$$\begin{aligned} G(-\infty) &= 1 \\ G(\infty) &= 3 \quad . \end{aligned} \tag{6.23}$$

The expected qualitative course for $G(x)$ at different volumes is shown in figure 6.2. The general class of functions to model the complete range of $G(x)$ are asymmetric sigmoidal ('s-shaped') functions where an appropriate infinite volume limit can be taken.

6.2.1 Polynomial fit

Probably the most straightforward way to proceed is expanding the function $G\left(tN_s^{y_t}\right)$ around $t = 0$ up to a certain order and then transforming to the variable κ via equation 6.16:

$$G\left(\left(\kappa - \kappa_{cp}\right) N_s^{y_t}\right) = \left(A + B\left(\kappa - \kappa_c\right) N_s^{y_t} + \dots\right) \tag{6.24}$$

The coefficients $A, B, \ldots$ are parameters to be determined by the fit. Demanding that $B_4(\kappa_c) = B_4(CP) = 1.604$ sets the constant $A = B_4(CP)$ so hat we have

$$G\left((\kappa - \kappa_c)\, N_s^{y_t}\right) = \left(B_4(CP) + B\,(\kappa - \kappa_c)\, N_s^{y_t} + \ldots\right) \tag{6.25}$$

In this thesis, polynomial fits up to order $\mathcal{O}\left(\left(\kappa - \kappa_{cp}\right)^3 N^{y_t 3}\right)$ were tried out.

Using a polynomial fit has certain restrictions. The asymptotic behaviour for the kurtosis discussed in the previous section can not be achieved using a polynomial fit as it will cross the boundaries eventually. Especially a linear fit can not describe the asymmetry around the critical point. Nevertheless the polynomial fit of first order can serve as a benchmark for a different fit when in the direct vicinity of the critical point. The value for κ at the critical point determined by another fit should coincide with the results from the linear fit.

6.2.2 Gompertz fit

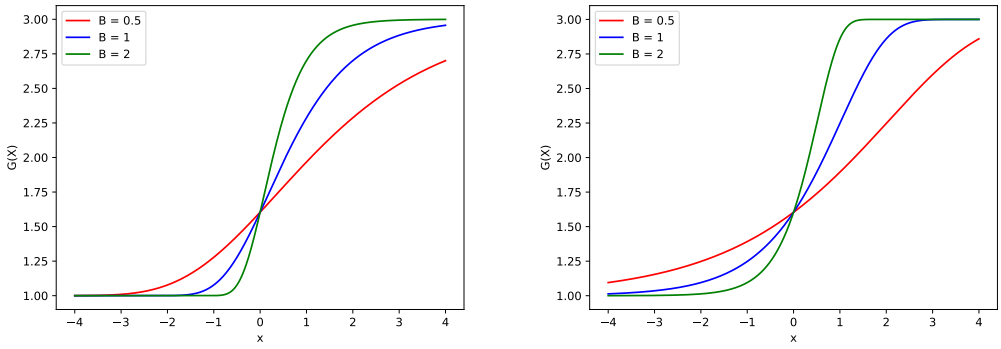

FIGURE 6.3: The two different ansätze arising from the gompertz function $G_g(x)$ (left) and $G'_g(x)$ (right) while the fitting parameter B is varied.

One possible ansatz that can fullfill the asymptotic behaviour is the Gompertz function. It is an asymmetrical sigmoidal function. A general form can be written as

$$G_g(x) = L + (U - L)e^{-Ae^{-Bx}} \quad . \tag{6.26}$$

Taking the limits $x \to \infty$ and $x \to -\infty$ reveals that L and U correspond to the lower and upper bound respectively so they can be set to $L = 1$ and $U = 3$ here. The constant A can be determined using the condition that $G(0) = B_4(CP) = 1.604$. Setting

$$A = -\ln\left(\frac{B_4(CP) - L}{U - L}\right) \approx 1.1973$$

leads to

$$\begin{aligned} G_g(0) &= L + (U - L)e^{\ln\left(\frac{B_4(CP)-L}{U-L}\right)} \\ &= L + B_4(CP) - LB_4(CP) \quad . \end{aligned} \tag{6.27}$$

Thus the fit ansatz using the gompertz function has the general form

$$G_g\left((\kappa-\kappa_c)\right) = L + (U-L)e^{\ln\left(\frac{B_4(CP)-L}{U-L}\right)e^{-B(\kappa-\kappa_{cp})N_s^{y_t}}} \tag{6.28}$$

with the two fitting parameters B and κ_{cp}. In addition to this, a similar ansatz is given by

$$G'_g(x) = U + (L-U)e^{-Ae^{Bx}} \quad . \tag{6.29}$$

This is identical to equation 6.26 only that U and L are swapped and $x \to -x$. It still has the correct behaviour that $\lim_{x\to-\infty} G(x) = 1$ and $\lim_{x\to\infty} G(x) = 3$, given that $U = 3$ and $L = 1$. The two functions differ in their symmetry around $G(0)$. Demanding $G(0) = B_4(CP)$ determines that

$$A = -\ln\left(\frac{B_4(CP)-U}{L-U}\right) = 0.3595 \quad .$$

This then gives the ansatz

$$G'_g\left((\kappa-\kappa_{cp})N_s^{y_t}\right) = U + (L-U)e^{\ln\left(\frac{B_4(CP)-L}{L-U}\right)e^{-B(\kappa-\kappa_{cp})N_s^{y_t}}} \tag{6.30}$$

with again two fitting parameters B and κ_c. The two different ansätze are pictured in figure 6.3.

6.2.3 General logistic fit

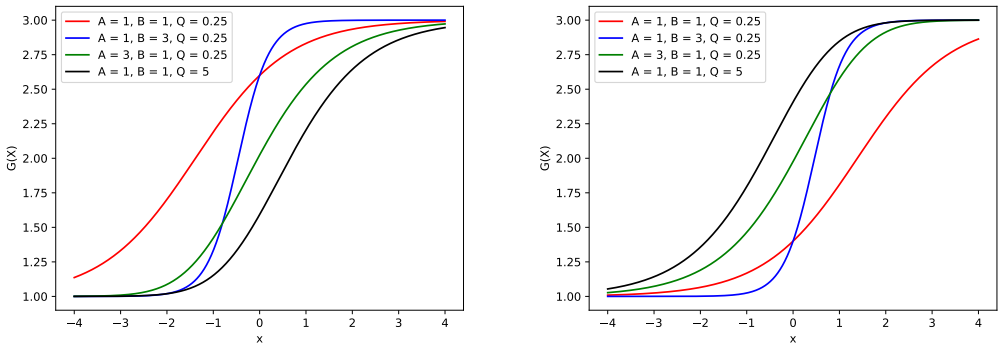

FIGURE 6.4: The general logistic function $G_l(x)$ (left) and the flipped version $G'_l(x)$ (right) for different parameters A, B, Q. Not pictured: $G''_l(x)$ from 6.43.

Another possible ansatz for $G(x)$ is the general logistic function given by

$$G_l(x) = L + \frac{U-L}{(1+Qe^{-Bx})^A} \quad . \tag{6.31}$$

Like the Gompertz function, the function is an asymmetric sigmoidal function. The parameters L and U describe the lower and upper bound respectively so that

$$G_l(-\infty) = L \quad ; \quad G(\infty) = U \quad . \tag{6.32}$$

Again, likewise to the Gompertz function a similar plot can be achieved by switching the parameters L and U and changing x to $-x$

$$G_l'(x) = U + \frac{L-U}{(1+Qe^{Bx})^A} \quad . \tag{6.33}$$

This again results in the same asymptotic behaviour while the symmetry around $G_l(0)$ is changed. Demanding that $G(0) = B_4(CP) = 1.604$ leads to

$$1 + Q = \left(\frac{U-L}{B_4(CP)-L}\right)^{\frac{1}{A}} \quad . \tag{6.34}$$

This means that either the parameter Q or A can be eliminated

$$Q = \left(\frac{U-L}{B_4(CP)-L}\right)^{\frac{1}{A}} - 1 \tag{6.35}$$

$$A = \frac{\ln\left(\frac{U-L}{B_4(CP)-L}\right)}{\ln(1+Q)} \tag{6.36}$$

Demanding $G_l'(0) = B_4(CP)$ leads to equations 6.35 and 6.36 only that U and L are switched

$$Q = \left(\frac{L-U}{B_4(CP)-U}\right)^{\frac{1}{A}} - 1 \tag{6.37}$$

$$A = \frac{\ln\left(\frac{L-U}{B_4(CP)-U}\right)}{\ln(1+Q)} \quad . \tag{6.38}$$

In total there are four possible ansätze resulting from the general logistic function

$$G_l\left(\left(\kappa-\kappa_{cp}\right)N_s^{y_t}, A\right) = L + \frac{U-L}{\left[1+\left(\left(\frac{U-L}{B_4(CP)-L}\right)^{\frac{1}{A}}-1\right)e^{-B(\kappa-\kappa_{cp})N_s^{y_t}}\right]^A} \tag{6.39}$$

$$G_l\left((\kappa-\kappa_{cp})N_s^{y_t}, Q\right) = L + \frac{U-L}{\left[1+Qe^{-B(\kappa-\kappa_{cp})N_s^{y_t}}\right]^{\frac{\ln\left(\frac{U-L}{B_4(CP)-1}\right)}{\ln(1+Q)}}} \tag{6.40}$$

$$G_l'\left(\left(\kappa-\kappa_{cp}\right)N_s^{y_t}, A\right) = U + \frac{L-U}{\left[1+\left(\left(\frac{L-U}{B_4(CP)-U}\right)^{\frac{1}{A}}-1\right)e^{-B(\kappa-\kappa_{cp})}N_s^{y_t}\right]^A} \tag{6.41}$$

$$G_l'\left(\left(\kappa-\kappa_{cp}\right)N_s^{y_t}, Q\right) = U + \frac{L-U}{\left(1+Qe^{-B(\kappa-\kappa_{cp})N_s^{y_t}}\right)^{\frac{\ln\left(\frac{L-U}{B_4(CP)-1}\right)}{\ln(1+Q)}}} \tag{6.42}$$

where the argument A signals that Q was expressed by A and vice versa. Each ansatz has three fitting parameters B, κ_c, Q/A.

In addition to the ansätze from equations 6.39 to 6.42 another ansatz G_{l2} similar to the general logistic function was tried. The function can be obtained by setting

$A = 1$ in the general form 6.31 and adding another exponential in the denominator

$$G_{l5}(x) = L + \frac{U - L}{1 + Q_1 e^{-B_1 x} + Q_2 e^{-B_2 x}} \quad . \tag{6.43}$$

Again, this has the required asymptotic behaviour. One of the parameters Q_1 and Q_2 can be eliminated from the requirement that $G_l''(0) = B_4(CP)$, leading to

$$Q_2 = \frac{U - L}{B_4(CP) - L} - 1 - Q_1 \quad . \tag{6.44}$$

Again, U and L can be switched if x is changed to $-x$. This finally gives the ansätze

$$G_{l5}\left(\left(\kappa - \kappa_{cp}\right) N_s^{y_t}\right) = L + \frac{U - L}{1 + Q_1 e^{-B_1 x} + \left(\frac{U-L}{B_4(CP)-L} - 1 - Q_1\right) e^{-B_2 x}} \tag{6.45}$$

$$G'_{l5}\left(\left(\kappa - \kappa_{cp}\right) N_s^{y_t}\right) = U + \frac{L - U}{1 + Q_1 e^{-B_1 x} + \left(\frac{L-U}{B_4(CP)-U} - 1 - Q_1\right) e^{-B_2 x}} \quad . \tag{6.46}$$

Chapter 7

Analysis of the data

7.1 General procedure

In generating and analyzing the data multiple steps were taken. The goal was to get a set of data points describing the kurtosis at different pairs of (τ_c, κ_c) near the suspected critical point for different values of N_s and then apply the fit ansätze derived in the last section. The critical point from the simulations done in [7] is located at $\kappa_{cp} = 0.016 \pm 0.02$. The complete procedure can be summarized as follows

1. Choose different values of κ near the critical point and simulate at different values of τ for each κ value. Do this at multiple values of N_s. Simulate many κ values in the direct vicinity of the critical point and only few values at greater distance.

2. For each κ, find the τ value at which the skewness becomes 0. This is the critical value τ_c for the given κ.

3. Plot the kurtosis at (τ_c, κ_c) versus κ and apply the different fit ansätze. Compare their results.

Besides determining the zero crossing of the skewness to find out the critical τ values, the susceptibility and kurtosis as a function of τ can be used as double check to verify or discard certain data points. As already discussed, the kurtosis should as-

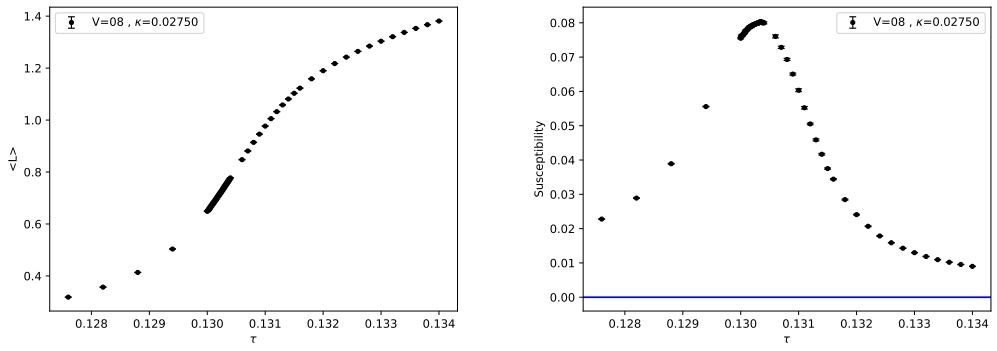

FIGURE 7.1: The order parameter $\langle L \rangle$ and the its susceptibility for varying τ at $N_s = 8$ (in the plot written as $V = 8$).

sume a local minimum when the skewness is equal to zero. The susceptibility of the order parameter $\langle L \rangle$ should be at a maximum. This is because the order parameter changes from 0 to a value greater than 0 when varying τ while the rate of change is

greatest at $\tau = \tau_c$. See figure 7.1 for a visualization. These additional criteria can be used to justify the exclusion of certain data points, even when the skewness is equal to 0. Another criterion to judge the quality for the nonlinear fits is given by the linear fit. A linear fit should be applied to the data points that are in direct vicinity of the critical point. The value of κ_{cp} calculated by a different fit should coincide with the value given by the linear fit. The same is true for the fitting parameter C in the general ansatz in equation 6.19 as it is not unique to the fit function applied. If this is not the case it can be taken as an indicator for the specific non-linear fit to not be applicable. Furthermore, when trying the non-linear fits it is important to keep in mind that the general ansatz derived in section 6.1

$$B_4 = G(tN_s^{y_t})(1 + CN_s^{y_t - y_h}) \tag{7.1}$$

was derived as an approximation close to the critical point. Since the non-linear fits will include data points that are not in the direct vicinity of the critical point it should be tested how the quality of a fit is affected when adding or removing data points that are further away from the critical point. It can not be assumed that the general ansatz gives reasonable results when moving away from the critical point.

7.1.1 Python fitting GUI

To analyze the data for the kurtosis the program 'Python fitting GUI' developed by Reinhold Kaiser in [4] was used. It can plot the data points and apply the various fitting functions discussed in section 6.2 to the data. Additionally, the quantities $\frac{\chi^2}{N_{DOF}}$ and Q are given. Due to an unknown bug in the program no fits following equations 6.40 and 6.42 could be calculated.

7.2 The data

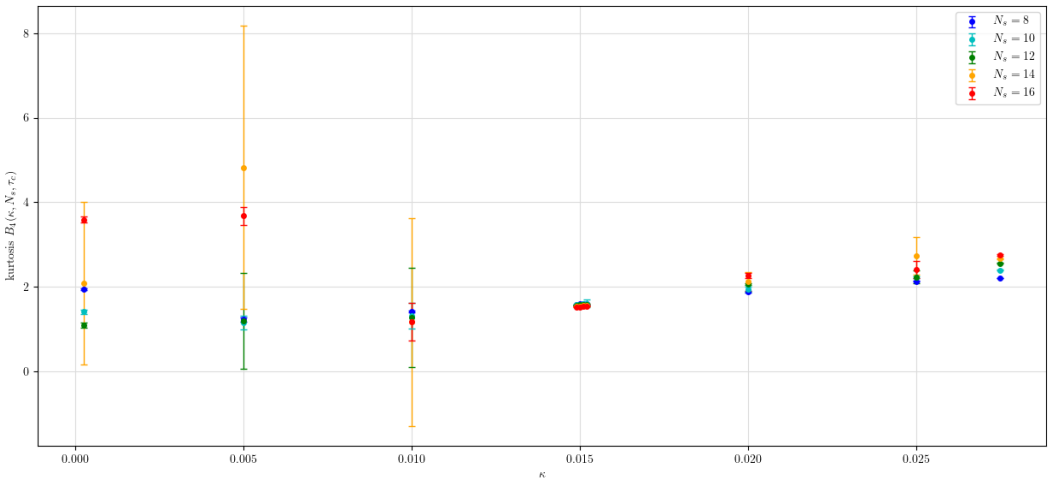

FIGURE 7.2: The kurtosis at (τ_c, κ_c) plotted against κ for different volumes.

.

The kurtosis data obtained from the simulations is shown in figure 7.2. The data in direct vicinity of the critical point is shown in figure 7.3. The plots show the kurtosis evaluated at (τ_c, κ_c) for different κ values. The simulations were run on five

different volumes with $N_s = 8, 10, 12, 14, 16$. The different κ values used are shown in table 7.1. All data points except those with $\kappa = 0.00025$ and $\kappa = 0.02750$ were

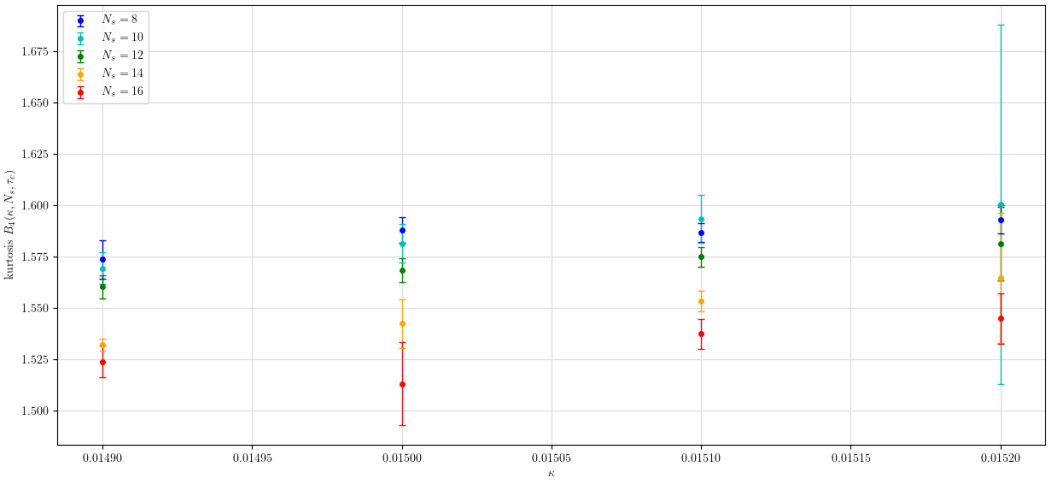

FIGURE 7.3: The kurtosis at (τ_c, κ_c) close to the critical point plotted against κ for different volumes.

.

$\kappa =$	0.00025	0.00500	0.01000	0.01490	0.01500
	0.01510	0.01520	0.02000	0.025000	0.02750

TABLE 7.1: The different κ values that were used.

previously generated and evaluated. For this thesis, only simulations with the two remaining κ values were carried out. In the simulations following the metropolis algorithm, $N = 100000$ measurements were taken for each observable. Between every measurement, N_s^3 updates in the Markov chain were carried out to avoid correlation of successive measurements. The first measurement was taken after $10 \cdot N_s^3$ updates. For the data seen in figure 7.2, τ_c was only determined by checking where the skewness is equal to 0. In table A.1 in appendix A the results from that analysis are shown. When additionally checking wether the kurtosis is minimized as well as checking if the susceptibility of the order parameter is maximized, some data points can be excluded. For $\kappa = 0.00025$ (the data points on the left side of the plot), all points can be discarded except for $N_s = 12$ as the additional criteria are not fulfilled. This is as well the case for $\kappa = 0.00500$ and $N_s = 14, 16$. When just judging the plot by eye, it is also reasonable to exclude these points as they defer from the expected behaviour greatly. The reason for this poor behaviour could be because the wrong zero-crossing of the skewness was analyzed for $\kappa = 0.00025$. The skewness in the complete range of τ values that were simulated is shown in figure 7.4 for $N_s = 8$ and $\kappa = 0.00025, 0.02750$. It can be seen that the curve for $\kappa = 0.00025$ only crudely resembles the curve for $\kappa = 0.02750$, where the data was acceptable. When viewing table A.1 and inspecting how much τ_c changes when varying κ it can be argued that for $\kappa = 0.00025$, τ should have been simulated around $\tau = 0.13600$. The values that were simulated covered a range around $\tau = 0.13700$. Because of these facts it is reasonable to assume that the zero crossing for $\kappa = 0.00025$ in figure 7.4 is not the zero crossing corresponding to the critical values. No further simulations could be performed so that the deadline of this thesis could've been met. Even though the

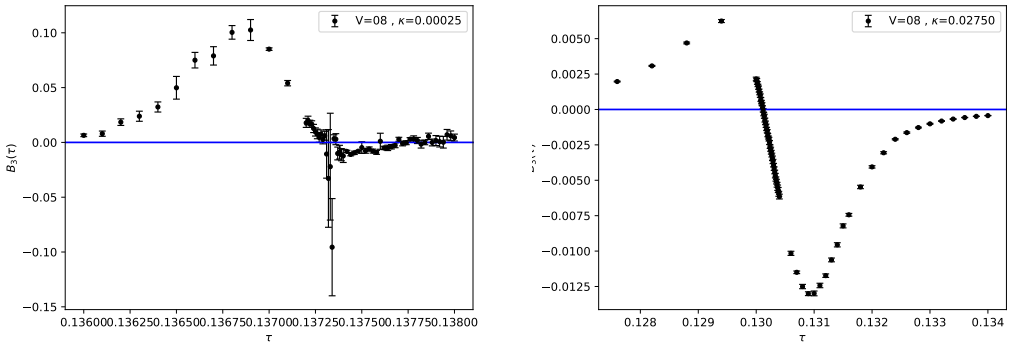

FIGURE 7.4: The skewness as a function of τ for $N_s = 8$ and $\kappa = 0.00025$(left) and $\kappa = 0.02750$ (right).

point at $N_s = 12$ where $\kappa = 0.00025$ satisfies the additional criteria given by the susceptibility and kurtosis as functions of τ, all points with $\kappa = 0.00025$ were excluded from the fits.

Instead of using the error for the kurtosis that was calculated during the simulation following the jacknife method, the error was determined by hand. This is to account for the fact that there is some error in determining τ_c from the zero crossing of the skewness. As the skewness was only calculated for discrete τ values, the true value at which the skewness becomes zero can not be determined. The error was estimated by comparing the kurtosis values at the estimated τ_c to the kurtosis values of the neighbouring τ. Between two consecutive τ values, τ was varied by 0.00001. Then if for example $\tau_c = 0.13326$, the cases $\tau = 0.13327$ and $\tau = 0.13325$ were considered. The error was then estimated as the difference of the kurtosis value at τ_c and the closest kurtosis value of one of the neighbours. For example, for $\kappa = 0.01500$ the kurtosis at τ_c was equal to $B_4 = 1.51316$. The closest neighbouring kurtosis value was equal to $B_4 = 1.53382$ (see figure 7.5). The error E was then estimated as $E = |1.51316 - 1.53382| = 2.66\dot{1}0^{-2}$. While this certainly leads to an overestima-

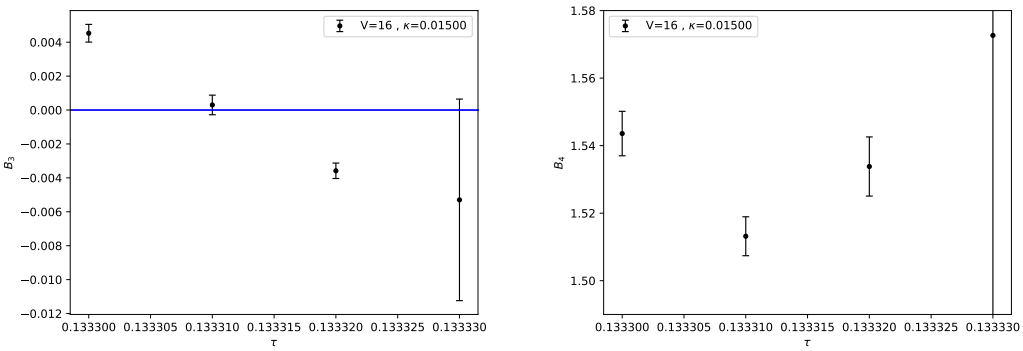

FIGURE 7.5: The skewness (left) and kurtosis (right) as a function of τ near the τ_c for $N_s = 16$ and $\kappa = 0.01500$.

tion of the error for some data points where the calculated kurtosis varies strongly around τ_c, the discussion of the linear fits will feature a justification of this approach.

7.3 The fits

All fits followed the general ansatz given in 6.19. The different possibilities for $G(x)$ were tried out. In all fits applied the inclusion of the correction term $(1 + CN_s^{y_t - y_h})$ lead to an improvement of the fit in the sense that $\frac{\chi^2}{N_{DOF}}$ was closer to 1 and Q was closer to 0.5 than if the term were not included. Only fits using this correction term will be presented. In what follows, C will always refer to the fitting constant C of the correction term. χ^2 will always refer to the quantity $\frac{\chi^2}{N_{DOF}}$.

7.3.1 Linear region

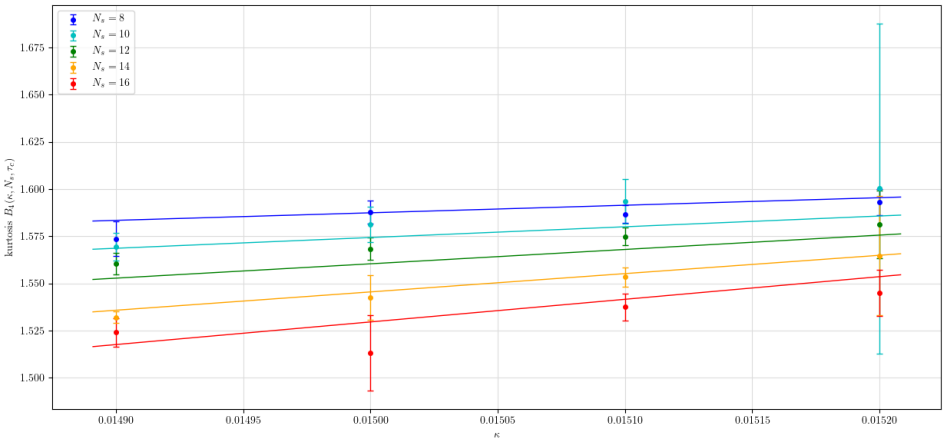

FIGURE 7.6: The results of the linear fit close to the critical point.

In figure 7.6 the linear fit applied to the data close to the critical point is pictured. It followed the general polynomial ansatz given in 6.25 up to the first order. The values for the fitting parameters are shown in table 7.2. The critical point value

κ_{cp}	χ^2	N_{DOF}	Q	C	B
0.01567(13)	0.8206	17	0.6706	0.040(16)	1.47(26)

TABLE 7.2: Fitting parameters for the linear fit. B refers to the first order polynomial coefficient.

$\kappa_{cp} = 0.01567 \pm 0.00013$ agrees with the result of $\kappa_{cp} = 0.16 \pm 0.2$ given in [7]. While the values for χ^2 and Q are acceptable, even better results are achieved by including the second and third orders of the polynomial fit ansatz to account for small deviations from a straight line. This leads to the plot seen in figure 7.7. The values of the fitting parameters are shown in table 7.3. The fitting parameters C_{fit} (not to be confused with C from the correction term) and D that give the second and third order polynomial coefficients were so small that the Python fitting GUI could not print out a result and showed an error message. No converging fit in the linear region could

κ_{cp}	χ^2	N_{DOF}	Q	C	B	C_{fit}	D
0.01567(15)	0.9300	15	0.5293	0.040(28)	1.5(6)	N.A	N.A.

TABLE 7.3: Fitting parameters for the polynomial fit in the linear region.

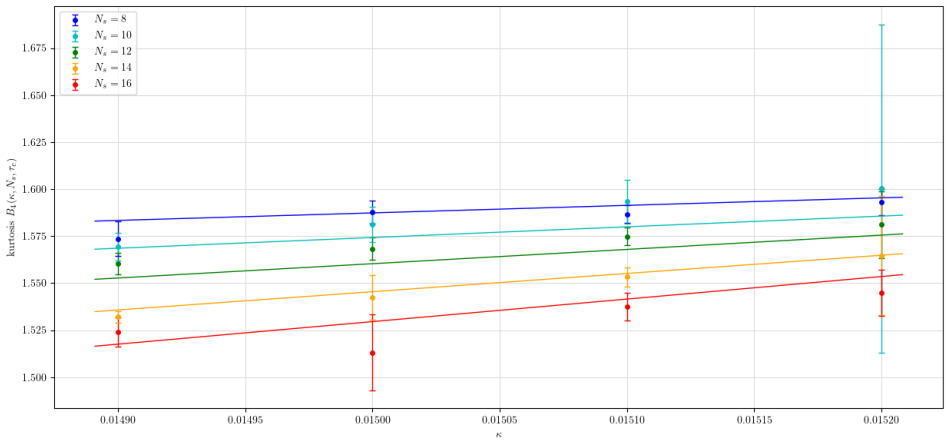

FIGURE 7.7: The results of the polynomial fit up to third order close to the critical point.

be achieved using one of the nonlinear ansätze.

Validity of the method to estimate errors

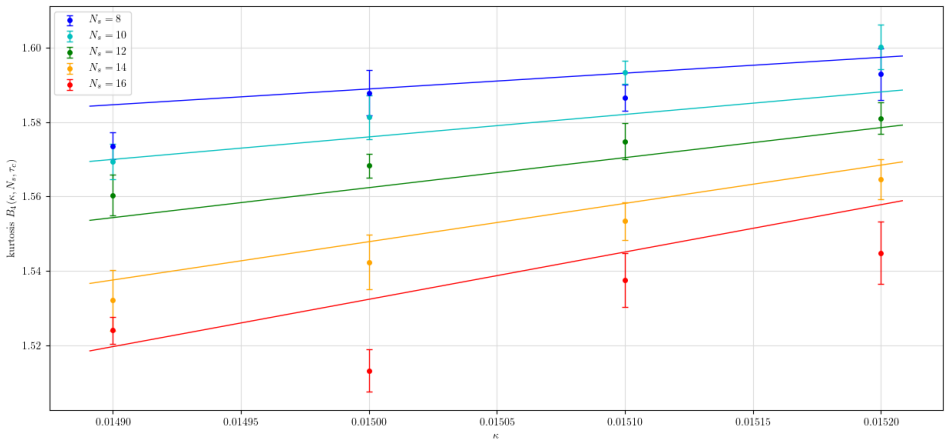

FIGURE 7.8: The results of the linear fit applied to the data using only the errors given by the simulation.

While the method of estimating errors presented in section 7.2 is far from rigorous, it lead to acceptable results for the linear fits. In 7.8 a linear fit is applied to the data that uses only the errors given by the simulation. The fitting parameters are shown in table 7.4. We can see that the fit is not performing well since $\chi^2 \approx 3$ and $Q = 0$.

κ_{cp}	χ^2	N_{DOF}	Q	C	B
0.01561(8)	3.3210	17	0	0.043(10)	1.56(16)

TABLE 7.4: Fitting parameters for the polynomial fit applied to the data using only the errors given by the simulation.

This is surprising at first because the different points are relatively close together and a linear fit should be possible. A possible explanation is that the determination of τ_c is not precise enough, creating an additional error for the kurtosis. This is not taken

into account when calculating the error during the simulation. Since a linear fit is expected to work for data points closely packed together, the method of estimating the error already presented was chosen, leading to an acceptable linear fit. This might overestimate some of the errors but overall gives better results.

7.3.2 Complete data set

Almost all of the fits tried for the complete data set did not get satisfying results with χ^2 way above 1 and $Q = 0$ or close to 0. The only fit that can at least be considered to be of good quality was given by the fit derived from the general logistic function $G_{l5}(x)$ given by equation 6.45. The plot is shown in figure 7.9. The fitting parameters are shown in table 7.5.

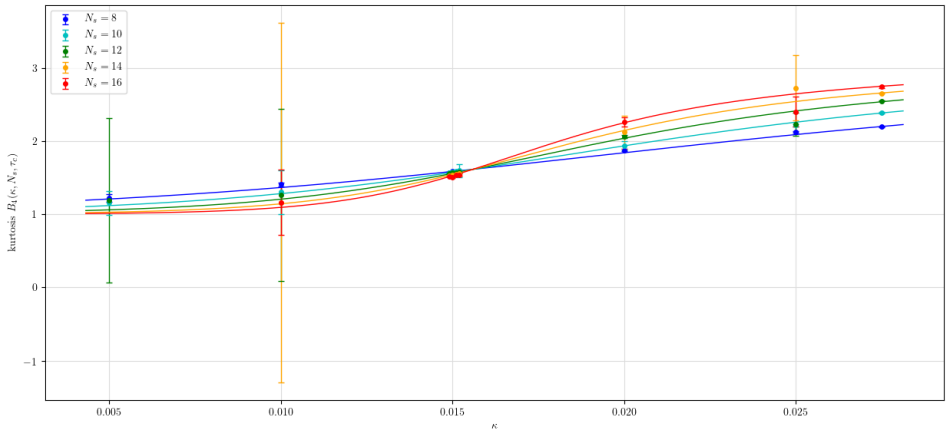

FIGURE 7.9: The results of the general logistic fit $G_{l5}(x)$ according to equation 6.45.

Fit	κ_{cp}	χ^2	N_{DOF}	Q	C	Q_1	B_1	B_2
$G_{l5}(x)$	0.01555(4)	1.2160	38	0.1694	0.045(15)	$17(3)10^3$	$0.7(22)10^{-5}$	1.7(3)
$G'_{l5}(x)$	0.01552(3)	2.1192	38	0	0.061(15)	$2(16)10^4$	1.00(19)	2.00(16)

TABLE 7.5: Fitting parameters for $G_{l5}(x)$ and G'_{l5} applied to the complete data set.

Fit	κ_{cp}	χ^2	N_{DOF}	Q	C	A	B
$G_l(x, A)$	0.01559(3)	2.6735	39	0	0.072(15)	$5(19)10^4$	2.4830(20)
$G'_{l5}(x, A)$	0.01641(5)	36.1843	39	0	0.279(15)	-10(4)	2.458(12)

TABLE 7.6: Fitting parameters for $G_l(x, A)$ and $G'_l(x, A)$ applied to the complete data set.

Although the value for κ_{cp} coincides with the linear fit, the values for χ^2 and Q are not optimal. Still, when comparing to the other fits, the function $G_{l5}(x)$ gives the best results. Table 7.6 shows the fitting parameters for the general logistic fitting functions $G_l(x, A)$ and $G'_l(x, A)$ from equations 6.39 and 6.41. The fitting parameters for the two gompertz fits $G_g(x)$ and $G'_g(x)$ are shown in table 7.7. Table 7.8 shows the fitting parameters for a first degree and third degree polynomial where the coefficient corresponding to $\left[(\kappa - \kappa_{cp})\, N_s\right]^2$ was set to 0 for the third degree polynomial.

Fit	κ_{cp}	χ^2	N_{DOF}	Q	C	B
$G_g(x)$	0.01559(3)	2.6066	40	0	0.072(15)	2.483(20)
$G'_g(x)$	0.01641(5)	35.2794	40	0	0.279(14)	2.458(12)

TABLE 7.7: Fitting parameters for $G_g(x)$ and $G'_g(x)$ applied to the complete data set.

Degree	κ_{cp}	χ^2	N_{DOF}	Q	C	B	D
1+3	0.015595(29)	2.5739	39	0	0.083(14)	1.821(14)	-0.912(9)
1	0.01623(3)	29.5442	40	0	0.343(12)	1.499(7)	N.A.

TABLE 7.8: Fitting parameters for a first degree and third degree polynomial applied to the complete data set.

7.3.3 Partial data set

The last set of points considered by removing data points on the outside of the complete data set so that only the points with $\kappa = 0.01000$, $\kappa = 0.02$ as well as the points near the critical point are included. For this data set, multiple fit ansätze turned out to provide a satisfying fit. Both versions of the Gompertz functions $G_g(x)$ and $G'_g(x)$ defined in equations 6.28 and 6.30 provided good results. Their plots can be see in figure 7.10 and 7.11. Another good fit was given by the general logistic function $G'_l(x, A)$ defined in equation 6.41. The plot can be seen in figure 7.12. The fitting parameters for the general logistic functions $G_l(x, A)$ and $G'_l(x, A)$ are presented in table 7.10. The fitting parameters for the general logistic fits $G_{l5}(x)$ and $G'_{l5}(x)$ can be seen in table 7.11. Finally, the fitting parameters for a first and third degree polynomial fit are pictured in table 7.12.

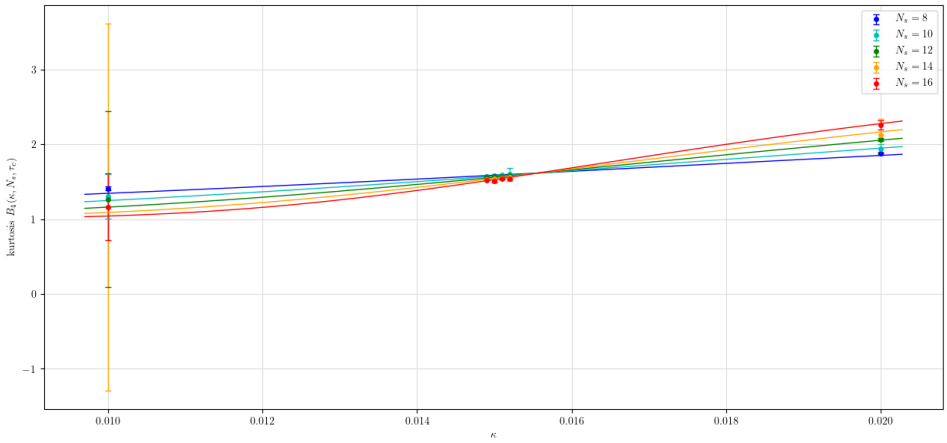

FIGURE 7.10: The results for the gompertz fit $G_g(x)$ according to equations 6.28.

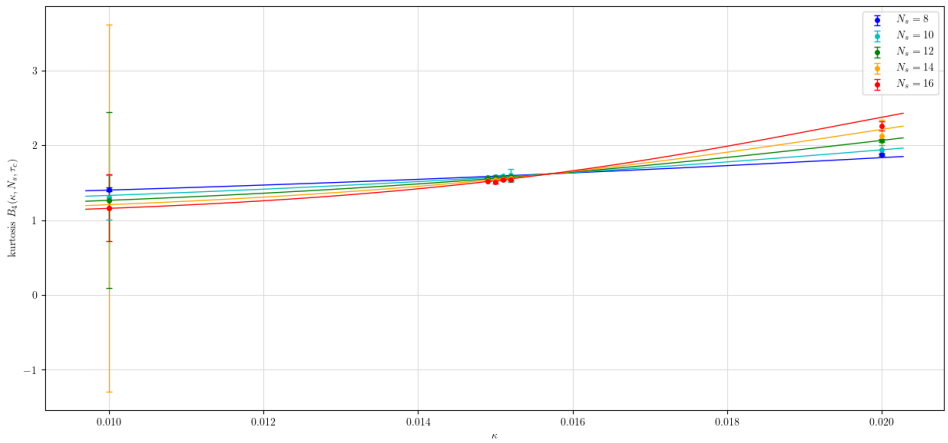

FIGURE 7.11: The results for the gompertz fit $G'_g(x)$ according to equations 6.30.

Fit	κ_{cp}	χ^2	N_{DOF}	Q	C	s
$G_g(x)$	0.01552(3)	0.9374	27	0.5571	0.045(15)	2.66(8)
$G'_g(x)$	0.01564(4)	0.9196	27	0.5840	0.0526(6)	3.27(8)

TABLE 7.9: Fitting parameters for the gompertz fits $G_g(x)$ and $G'_g(x)$ on the partial data set.

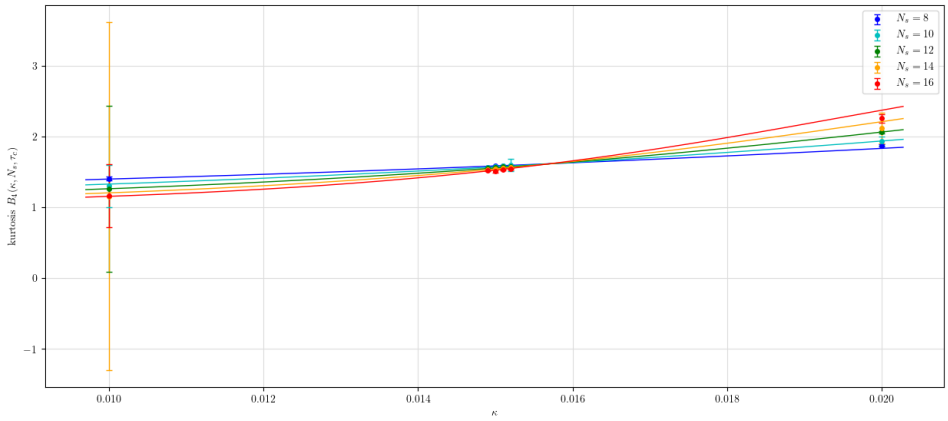

FIGURE 7.12: The results of the fit $G'_l(A)$ according to equation 6.41

Fit	κ_{cp}	χ^2	N_{DOF}	Q	C	B	A
$G_l(x, A)$	0.01558(5)	0.8069	26	0.7431	0.048(16)	0.40(10)	1.2(8)
$G'_l(x, A)$	0.01564(3)	0.9550	26	0.5286	0.052(24)	0.327(8)	$6(25)10^4$

TABLE 7.10: Fitting parameters for the general logistic fits $G_l(x, A)$ and $G'_l(x, A)$ on the partial data set.

Fit	κ_{cp}	χ^2	N_{DOF}	Q	C	B_1	B_2	Q_1
$G_{l5}(x)$	0.01556(5)	0.7735	25	0.78705	0.047(16)	$2.309(22)10^{-5}$	0.43(4)	$-11(24)10^4$
$G'_{l5}(x)$	0.01558(5)	0.8402	25	0.8402	0.048(16)	0.1(25)	10(10)	$10(11)10^6$

TABLE 7.11: Fitting parameters for the general logistic fits $G_{l5}(x)$ and $G'_{l5}(x)$ on the partial data set.

Degree	κ_{cp}	χ^2	N_{DOF}	Q	C	B	D
1+3	0.01551(4)	1.2016	27	0.2194	0.045(15)	1.93(9)	-1.0(6)
1	0.015523(3)	1.1689	27	0.2488	0.046(15)	1.89(5)	N.A.

TABLE 7.12: Fitting parameters for the first and third degree polynomial fits on the partial data set.

7.3.4 Discussion

Depending on the subset of data that was considered, more or less successful fits could be found when judging by χ^2 and Q. The best fits were those that contained data points closer to the critical point. This does not come as a surprise, since the general fit ansatz was derived in the vicinity of the critical point. Nevertheless, even for the complete data set a satisfying fit resulted from a general logistic function ansatz. Perhaps unsurprisingly, a fit being satisfactory according to χ^2 and Q also meant that the fit agreed with the κ_{cp} and C values predicted by the linear fit, which also agrees with the previously performed simulations in [7]. Remarkably, even some fit functions with relatively high values for χ^2 around $\chi^2 \approx 2$ and $Q \approx 0$ agreed with the predicted κ values. For the partial data set, multiple fitting ansätze proved to be of use. At least for this thesis, an asymmetrical sigmoidal fit ansatz proved to be a valid method to determine κ_{cp} when considering data further away from the critical point.

Chapter 8

Conclusion

In this thesis the κ value at the critical point for $\mu = 0$ in the Polyakov-loop model was determined. This was done by calculating the kurtosis at critical τ values for multiple values of κ and applying various fitting functions to the data. The thesis covered relevant background information including phase transitions, a brief introduction to the Renormalization group formalism, the skewness and kurtosis, the metropolis algorithm and an overview over fitting. Although not all data points simulated were usable, enough data was available to test out the fit functions. The original data lead to fits of bad quality due to a possible underestimation of the errors, a manual way to estimate the errors was introduced which gave an improvement. The fit functions were tried on different data sets containing or excluding points further away from the critical point. For each data set, at least one fit ansatz provided κ values agreeing with the linear fit, which was used a benchmark. The predicted κ values also agreed with results from different simulations. All in all, the method of fitting the kurtosis to a data set including points not in the direct vicinity of the critical point proved successful, at least for the Polyakov-loop model considered here. It might be useful to try similar ansätze for different models.

Appendix A

Values of τ_c

N_s	κ	τ_c	N_s	κ	τ_c
8	0.00025	0.13731	8	0.01510	0.13329
10	0.00025	0.13718	10	0.01510	0.13329
12	0.00025	0.13714	12	0.01510	0.13328
14	0.00025	0.13709	14	0.01510	0.13328
16	0.00025	0.13699	16	0.01510	0.13328
8	0.00500	0.13590	8	0.01520	0.13326
10	0.00500	0.13590	10	0.01520	0.13326
12	0.00500	0.13590	12	0.01520	0.13326
14	0.00500	0.13590	14	0.01520	0.13326
16	0.00500	0.13590	16	0.01520	0.13326
8	0.01000	0.13460	8	0.02000	0.13200
10	0.01000	0.13460	10	0.02000	0.13200
12	0.01000	0.13460	12	0.02000	0.13200
14	0.01000	0.13460	14	0.02000	0.13200
16	0.01000	0.13460	16	0.02000	0.13200
8	0.01490	0.13334	8	0.02500	0.13080
10	0.01490	0.13334	10	0.02500	0.13080
12	0.01490	0.13334	12	0.02500	0.13080
14	0.01490	0.13333	14	0.02500	0.13080
16	0.01490	0.13333	16	0.02500	0.13080
8	0.01500	0.13332	8	0.02750	0.13012
10	0.01500	0.13332	10	0.02750	0.13011
12	0.01500	0.13331	12	0.02750	0.13011
14	0.01500	0.13331	14	0.02750	0.13011
16	0.01500	0.13331	16	0.02750	0.13010

TABLE A.1: The values for τ_c obtained from analysis of the skewness for different values of N_s and κ.

Bibliography

[1] C.B. Lang C. Gattringer. *Quantum Chromodynamics on the Lattice*. 2010.

[2] John Cardy. *Scaling and Renormalization in Statistical Physics*. 1996.

[3] Nigel Goldenfeld. *Lectures On Phase Transitions And The Renormalization Group*. 1998.

[4] Reinhold Kaiser. *Locating the Heavy Z_2 Point in $N_f = 2$ LQCD at Zero Chemical Potential*. 2020.

[5] F Karsch, E Laermann, and Ch Schmidt. "The chiral critical point in 3-flavour QCD". In: *Physics Letters B* 520.1 (2001), pp. 41–49. ISSN: 0370-2693. DOI: https://doi.org/10.1016/S0370-2693(01)01114-5. URL: https://www.sciencedirect.com/science/article/pii/S0370269301011145.

[6] Jangho Kim et al. "The SU(3) spin model with chemical potential by series expansion techniques". In: *JHEP* 10 (2020), p. 051. DOI: 10.1007/JHEP10(2020)051. arXiv: 2007.04187 [hep-lat].

[7] Ydalia Delgado Mercado and Christof Gattringer. "Monte Carlo simulation of the SU(3) spin model with chemical potential in a flux representation". In: *Nuclear Physics B* 862.3 (2012), 737–750. ISSN: 0550-3213. DOI: 10.1016/j.nuclphysb.2012.05.009. URL: http://dx.doi.org/10.1016/j.nuclphysb.2012.05.009.

[8] Shinji Takeda et al. *Update on Nf=3 finite temperature QCD phase structure with Wilson-Clover fermion action*. 2016. arXiv: 1612.05371 [hep-lat].

[9] Peter Young. *Data Analysis and Fitting for Physicists*. 2012.

List of Figures